V2G Dynamic Headroom Control

Initial Simulation Study

Version 1.0

11th June 2025

Prepared by:

Andrew Urquhart and Murray Thomson

CREST, Loughborough University

Prepared for:

Liza Troshka

National Grid Electricity Distribution

Contents

1. Introduction 3
2. Network models 4
   2.1 Network data 4
   2.2 Cable impedances 6
   2.3 Customer demand 7
      2.3.1 Conventional appliances 7
      2.3.2 DFES estimates of LCT uptake 7
      2.3.3 Heat pumps 8
      2.3.4 Solar PV 8
      2.3.5 EV chargers 8
      2.3.6 V2G EV chargers 12
      2.3.7 Volt-watt control 12
      2.3.8 Volt-var control 13
      2.3.9 Application of volt-watt and volt-var control 14
   2.4 Simulation configuration 14
3. Results for sample substation 892320 16
   3.1 Volt-watt control 16
   3.2 Volt-watt control with diversified recharging 18
   3.3 Volt-var control 19
4. Results for selected substations 21
   4.1 Baseline 21
   4.2 Added LCTs 22
   4.3 V2G 23
   4.4 Volt-watt V2G 24
   4.5 Volt-var V2G 25
   4.6 V2G with diversified recharging 26
   4.7 Volt-watt V2G with diversified recharging 27
   4.8 Volt-var V2G with diversified recharging 28
5. Summary results 29
   5.1 Maximum voltage 29
   5.2 Minimum voltage 31
   5.3 Cable loss powers 32
   5.4 Maximum RMS currents per feeder 33
   5.5 Mains branches with current overload 34
6. Conclusions 35
7. References 36

1. Introduction

This report summarises results from an initial modelling exercise intended to assess control techniques that mitigate voltage rise due to power exported to the grid from electric vehicle batteries.

The modelling considers the development of low carbon technologies (LCTs) on low voltage (LV) substation and LV feeders. An initial baseline model considers the LV feeders with existing demands, followed by a second model where solar photovoltaics (PV), heat pumps and electric vehicles (EVs) are added. This model uses the distribution future energy scenarios (DFES) to estimate a likely uptake of these appliances for a selected future year of 2035.

The model then adds vehicle-to-grid (V2G) operation, taking an extreme assumption that all EV chargers participate in an export event, such as might be arranged via a supplier or aggregator to support a sudden loss of generation, or the loss of an interconnector, on the wider grid. It is assumed that every EV charger has a vehicle connected such that power can be supplied back to the grid. This event is timed in the early afternoon when exports from solar PV are already high and demand from other appliances will be lower.

Volt-watt and volt-var control techniques are then added to determine their impact on the maximum and minimum voltage ranges and on the thermal loading of the LV feeders. Volt-watt control shows significant reductions in the voltage rise caused by V2G, although this is achieved at the expense of limiting exports. WP2 will consider how the control techniques can optimise the benefits from the network perspective, while maintaining the maximum possible exports to support the wider grid, taking into account the headroom indicated by the smart meter data. The volt-var control method provides less reduction in the voltage rise, but has the advantage that the exported power is largely unaffected.

Section 2 of this report describes the process used to import network data from an NGED Electric Office database, and to combine with the locations of customer connections, Section 2.2 describes the method used to define cable impedances, and approximations that have been made due to the lack of more detailed reactance data for each cable type. Future simulations will be able to use more accurate data available from NGED.

Section 2.3 describes the methods used to synthesize customer demand data. In future work this will partly be replaced by data from smart meters, but the use of fully synthetic data has allowed greater flexibility in the modelling as the demand data can be modified as required.

Results of the modelling for one example substation are shown in section 3, where some of the mechanisms that cause the worst-case voltage rise and voltage drops are explored.

A summary of simulations from across the set of selected substations is shown in section 4.

2. Network models

2.1 Network data

The process for importing network data from the NGED Electric Office database has been developed previously for the Parc Eirin project. Details of this process are summarised again here, with revisions to account for changes to the method for this project.

Electric Office mapping data for the LV network has been provided in four `sqlite` files, one for each NGED license area.

Networks data has been imported for a set of LV substations identified for this project in the Site Selection Report [1].

The databases contain a number of tables, many of which are not required in this modelling work. Fields that have been utilised are as follows.

Table 1: Electric Office database tables

Table	Geometry	Content
cable	Line	Underground cables
wire	Line	Overhead lines
connector_segment	Line	Zero impedance connectors that are shown on the GIS diagram to show topological links between cables, wires, and isolating equipment
substation_gm	Polygon	Ground-mounted substations
substation_pm	Point	Pole-mounted substations
service_point	Point	Locations on the network edge that provides a connection to a customer
service_connection	service_point	Customer MPANs that are linked to service points

The modelling software treats all cables and wires as branch records, and both ground-mounted and pole-mounted substations as substation records.

The features defined with a line geometry have an associated circuit id field that identifies the substation and LV feeder. The modelling software assumes that these have been defined correctly within the Electric Office system, such that there is no further need to 'crawl' through the network and find cables that have topological connections to each other.

Previous work on the Network Innovation Allowance (NIA) Losses Investigation and SMITN projects has demonstrated that customer connection records in CROWN are often inaccurate. The method here therefore uses a set of customers for which the selected LV feeders are the nearest, based on the Electric Office network diagram. Electric Office does not record the feeder connections for individual customers, so this is strictly only included in the database where the service cable is included in the diagram. For all other customers, the association is implied by proximity of the customer coordinates to the feeder main but not actually recorded in the data.

Branch records for cables and wires both include a definition of the geographic route, specified as a list of coordinate points. The lengths between each of these points are referred to here as segments, such a branch with N coordinate points will have $N - 1$ segments.

An input data file is therefore used to define MPANs for which the selected substation is the nearest. This file has been prepared previously and provides the identifier of the nearest branch, the nearest segment of the branch, and the coordinates of the nearest point on the branch with a tangential route to the MPAN location. This nearest point may be at one of the coordinate points used to define the branch route but more often will be an interpolated point between the two coordinates at either end of a branch segment.

The software creates the LV feeder topology for a selected substation as follows.

1. The substation coordinates are defined, either using the point location provided for a pole-mounted transformer, or the mean value of the boundary line defined for a ground-mounted transformer.
2. Branch records are selected, either cables or wires, where the substation id part of the circuit id matching the selected substation.
3. For each feeder, the software finds the nearest end point to the substation on the nearest cable or wire branch.
4. Connector records are selected, either cables or wires, where the substation id part of the circuit id matching the selected substation.
5. A dictionary is created for each branch end-point, containing a list of the branches that terminate at that point.
6. A dictionary is created for each service point record, containing the branch end-point at which it is located. If service points don't match any of the branch end-points then they are excluded at this stage.
7. A dictionary is created for each MPAN, containing the service point record at which it is located. If there is no service point record found, then the MPAN is excluded at this stage.
8. Customer nodes are created for each of the coordinates with an MPAN, and customer records are associated with these nodes.
9. Service cables be drawn in the network diagram mostly have an end-point at the feeder main that coincides with one of the coordinates on the route of the feeder main. These points may be within the geographic route of the feeder main branch, rather than at end-points. The mains branches therefore need to be split into shorter sections with new end-points at coordinates where service cables need to connect. The software identifies coordinate points that appear in the routes of multiple branches and where the point is not and end-point of one or more of the branches.
10. The process above defines locations for MPANs that have service connections shown in the Electric Office network diagram. A list of MPANs is then created that are associated with the substation but not yet connected as above. Generally, this will be the case for the majority of MPANs.
11. For each MPAN that has no connection drawn in the network diagram, the software finds the nearest branch and builds up a list of points where the feeder main will need to have a new junction inserted.
12. The feeder mains are then split into multiple shorter sections at these new junction points so that there are branch end points where the service cables can be connected.
13. The software then creates branch objects for each of the feeder main and service cable sections that have been defined.
14. Zero impedance branches are also created for any connector segments, other than those that join to the feeder mains at their nearest point to the substation. This allows for sections of the LV feeder that are joined across link-boxes to be included. The software developed so far does not check the status of isolators at the link-boxes but relies on the circuit ids having been appropriately identified such that all the required branches are included. The connector segments are therefore required such that branches beyond a link-box will not be islanded.
15. Having fully defined the branches and nodes for the selected network, the software builds the radial tree structure of each LV feeder, beginning with the node nearest the substation.

The LV feeder models may not be exactly correct, as customers are not always connected to their nearest feeder main, but the topologies can be considered as models that are close to the actual designs and representative of feeders that could plausibly exist.

Branches are created with a WinDEBUT cable type that defines the impedance matrix. These cable type definitions use different line codes to those in Electric Office and so a look-up table has been manually created. This includes the line codes that have been encountered for the substation circuit ids examined so far.

Where new service cables are added in the model, these are created using the Waveform 'WC 35' line code defined for Connect-LV library of cable impedances.

Customer connections have a phase rotation applied such that successive meters have phases of L1, L2, L3, then L2, L3, L1, and L3, L1, L2. Where customers have single-phase connections, the first of the corresponding three-phase rotation is selected. Three-phase appliances have one third of their demand power on each phase.

2.2 Cable impedances

Two alternative sets of impedance data have been used for this work. Initial simulations used impedances defined for WinDEBUT and only include the resistance term. Subsequent simulations, used for the main results in section 4, use revised impedance data defined for use with the Connect-LV software [2]. These include both the resistance and reactance terms of the cable impedances.

Cable impedances are specified in the model in terms of a 3×3 phase impedance matrix Z_{abc}, as used to calculate a voltage drop along the cable for a given phase current vector I_{abc}. Voltage drops are then calculated as

$$\Delta V_{\mathrm{abc}} = Z_{\mathrm{abc}} \cdot I_{\mathrm{abc}}$$

With individual phase currents and voltages annotated this becomes

$$\begin{pmatrix} \Delta V_{\mathrm{L1}} \\ \Delta V_{\mathrm{L2}} \\ \Delta V_{\mathrm{L3}} \end{pmatrix} = \begin{pmatrix} Z_{\mathrm{aa}} & Z_{\mathrm{ba}} & Z_{\mathrm{ca}} \\ Z_{\mathrm{ab}} & Z_{\mathrm{bb}} & Z_{\mathrm{cb}} \\ Z_{\mathrm{ac}} & Z_{\mathrm{bc}} & Z_{\mathrm{cc}} \end{pmatrix} \cdot \begin{pmatrix} I_{\mathrm{L1}} \\ I_{\mathrm{L2}} \\ I_{\mathrm{L3}} \end{pmatrix}$$

In the first case, where no reactance is defined for the cable impedance, a standardised reactance has been added for each cable type. This has been derived from finite element impedance models developed for the Losses Investigation project, where the reactance was found to be similar for Waveform cables of different sizes, ranging from 95 mm^2 to 300 mm^2.

As an approximation to represent the undefined reactive terms, a self-impedance reactive term of $0.07j$ Ω/km is Z_{aa}, Z_{bb}, and Z_{cc}. A mutual-impedance reactive term of $0.01j$ Ω/km is added to all the other off-diagonal terms in the matrix.

The impedances can also be expressed in terms of a sequence impedance matrix. The corresponding reactance of the positive sequence term is then $0.058j$ Ω/km. This would correspond to the 'star reactance' defined in cable impedance data tables. The zero sequence reactance is then $0.087j$ Ω/km.

In the later simulations using revised impedances for the Connect-LV software, the resistance and reactance terms are defined for the phase and neutral conductors. This data provides resistance and reactance values for the phase and neutral conductors. Combining the resistance and reactance terms, this gives a phase conductor impedance Z_{p} and a neutral conductor impedance Z_{n}.

In the absence of further information specifying the mutual impedances, these are assumed to be zero. The 3×3 phase impedance matrix Z_{abc} is constructed from solely from the phase and neutral conductor impedances, as follows:

$$Z_{\mathrm{abc}} = \begin{pmatrix} Z_{\mathrm{p}} + Z_{\mathrm{n}} & Z_{\mathrm{n}} & Z_{\mathrm{n}} \\ Z_{\mathrm{n}} & Z_{\mathrm{p}} + Z_{\mathrm{n}} & Z_{\mathrm{n}} \\ Z_{\mathrm{n}} & Z_{\mathrm{n}} & Z_{\mathrm{p}} + Z_{\mathrm{n}} \end{pmatrix} alpha$$

The impedance data from SD5H is defined for a set of line codes used in Connect-LV, but not including all of the line codes found within the network data in Electric Office. A lookup table provided by NGED defines appropriate 'best match' or equivalent cable types for many of the additional line codes, but some branches remained undefined. These have been assigned to corresponding cable types within the V2G simulation code.

2.3 Customer demand

2.3.1 Conventional appliances

For the purposes of this modelling, all the connections are assumed to be domestic customers, avoiding the need to import Durabill data for any half-hourly metered customers which has not been made available for this project. The selected substations typically have long rural lines or customers with a high proportion of domestic low carbon technologies so it is unlikely that many larger commercial customers will be connected.

Data from CROWN is used to define the Estimated Annual Consumption (EAC) for each customer. Where EACs are undefined they are assumed to be 3,509 kWh per annum [3]. The Elexon profile class is used where this is known or otherwise assumed to be Elexon profile class 1 (Domestic unrestricted customers on single-rate tariff).

Demand profiles are created at 1-minute resolution but values are the same for each of the 30-minute samples within a half-hourly period in the Elexon profile.

2.3.2 DFES estimates of LCT uptake

Additional demand data has been added to represent the LCTs, including solar PV, electric vehicle charging, and heat pumps. Numbers of these appliances are defined by scenarios in the Distribution Future Energy Scenarios (DFES) [4]. Data file 'DFES Volume Projections by Electricity Supply Area' has been downloaded, providing forecasts for three different scenarios, from which 'Electric Engagement' data has been selected.

It was previously expected that DFES data would be obtained for one location in each license area, but recently updated scenarios now provide data that is specific to each primary substation. CROWN customer records that list both the distribution and primary substation for each customer connection have been used to identify the primary for each distribution substations, such that the appropriate DFES scenario data can be selected. Forecast data for 2035 using the 'Electric Engagement' scenario has been selected for the analysis, other than for the baseline case where no additional LCTs are included.

Each DFES scenario provides numbers (or installed capacity) of LCTs and an estimated increase in population. The existing population has been estimated based on the number of MPAN connections to the primary in the CROWN data. Using these two figures, a population growth ratio can be calculated.

It is assumed that this applies uniformly over the distribution substations connected to the primary. Numbers of LCTs are assumed to be evenly spread across all the distribution substations connected to the primary. The number of LCTs is then calculated pro rata relative to the proportion of customers at each distribution substation, relative to the number of customers at the primary.

To serve the increasing population, it is assumed that additional substations and LV feeders would be connected to the network, and not that there would be additional customers connected to the existing LV feeders. The DFES estimates of LCT uptake allow for increased numbers of customers, and so

the numbers of LCTs on each existing feeders is divided by the population growth ratio. In effect, the population growth ratio reflects an increased number of LCTs due to an increased number of LV feeders, rather than an increasing number of customers on the existing LV feeders.

2.3.3 Heat pumps

Heat pumps are modelled as having a thermal power rating of 8 kW consistent with an air-source design based on an approximate average of installations for which data has been made available through the Renewable Heat Premium Payment scheme [5]. A COP factor of 3 has been assumed, such that the electrical power of the heat pumps is 2.67 kW. The annual heating demand is then approximated by taking the mean domestic gas demand of 12,000 kWh [6] multiplied by a boiler efficiency of 0.9, giving a total of 10,800 kWh. It is then assumed that two thirds of this is required for space heating and the remaining one third is used for domestic hot water. Both these thermal demands are then divided by the COP to find the annual electrical demand for space heating and for domestic hot water. As with previous Parc Eirin models, the domestic hot water demand follows a daily profile based on empirical data [7]. The space heating demand is assumed to be uniform throughout the day but with the daily demand weighted in proportion to a degree-day figure relative to 15.5 °C. Degree-day data has been used for Northampton, available from Stark [8]. At present the same degree-day data is used for each selected substation, making an approximation that local differences in temperatures will not significantly affect the outcome of the V2G models.

The model synthesizes heat pump demand data with 1-minute resolution. The model for each MPAN begins assuming a randomised ‘state of charge’ of hot water heat and of the space heating. In each successive minute, the hot water state of charge is decremented by a value that follows the hourly hot water demand profile. Similarly, the space heating state of charge is decremented by a value representing the daily heat requirement, based on the degree-day data. When either of these two states of charge reach zero, the model switches the heat pump on for a period of 10 minutes, followed by a pause between cycles of 5 minutes. This algorithm models an idealised heat pump operation where the heat is delivered ‘long and low’, with periods of operation evenly spread throughout the day rather than following a more traditional daily profile observed for gas heating.

2.3.4 Solar PV

PV systems are assumed to have a 3 kW rated power, an azimuth angle selected from a uniform distribution between 90° and 270°, and a tilt of 40°. Irradiance data is common to all houses at the substation and uses irradiance data and cloud shading model developed for the CREST demand model [9], [10]. At present the model uses common irradiance data for Milton Keynes at 52.04° latitude and -0.76° longitude for all substations. This could be refined to use more local data but, given the uncertainty in the number of PV systems deployed, it is not expected that this would significantly increase the overall accuracy.

The model synthesises 1-minute data for the PV output, allowing for variations in solar azimuth and elevation, and also short-term variations in the cloud cover.

At present there is no battery storage included in the model.

2.3.5 EV chargers

EV charger operation is modelled using empirical data from the NIA Electric Nation project. Samples are taken from probability distributions that represent the likely start time during the day, the number of charges per day (less than one), and the length of each charging session. For any one customer, the probability of chargers per day remains the same for the whole yearly period whereas the charging energy is reset for each session. These sampling methods were combined to give a reasonably close match to the observed probability distribution for the total EV charging demand per year.

The Electric Nation trials monitored home charging behaviour on a sample of approximately 670 participants with a wide range of plug-in vehicle types. Within this total, measurements have been selected here for battery capacities of 35 kWh or above, so that the modelling is as representative as possible of future vehicle types.

It has been assumed that the EV chargers will operate as a single-phase appliance and with a rated import power of 7 kW. In practice some customers may have smaller chargers of 3.68 kW but the higher rating of 7 kW appears to be commonplace.

The trials monitored the daily charging behaviour for up to two years, recording the plug-in time, the time when charging started, the energy delivered per session, and the total annual energy demand. This data is summarised as empirical statistical distributions in the trials report [11].

It has been assumed here that the demand per charging session and the number of charges per day can be represented by Weibull distributions, with shape factor α and scale parameter β selected to give a close approximation to the measured distributions [12], and also to be consistent with the mean annual demand of 3,430 kWh observed in the original measurement data.

Separate distributions have been fitted to the energy delivered per charging session, as in Figure 1, and for the number of charges per day, as in Figure 2. The parameters for the Weibull distributions were scaled such that the median and mean values are as close as possible to the box and whisker diagrams, with 25% and 75% values also being near to the given figures. An exact match for all parameters is not possible, obviously indicating that the original data distributions did not follow the Weibull mathematical shape. However, given the more significant approximations involved elsewhere in relation to the number of EVs and charging requirements, these remaining differences are not considered significant.

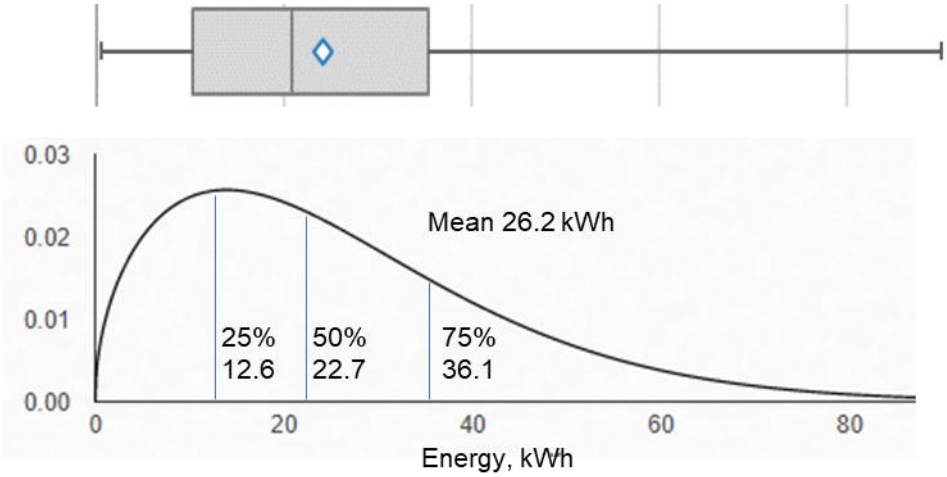

Figure 1: Energy delivered per charging session, [11] Figure 8-18

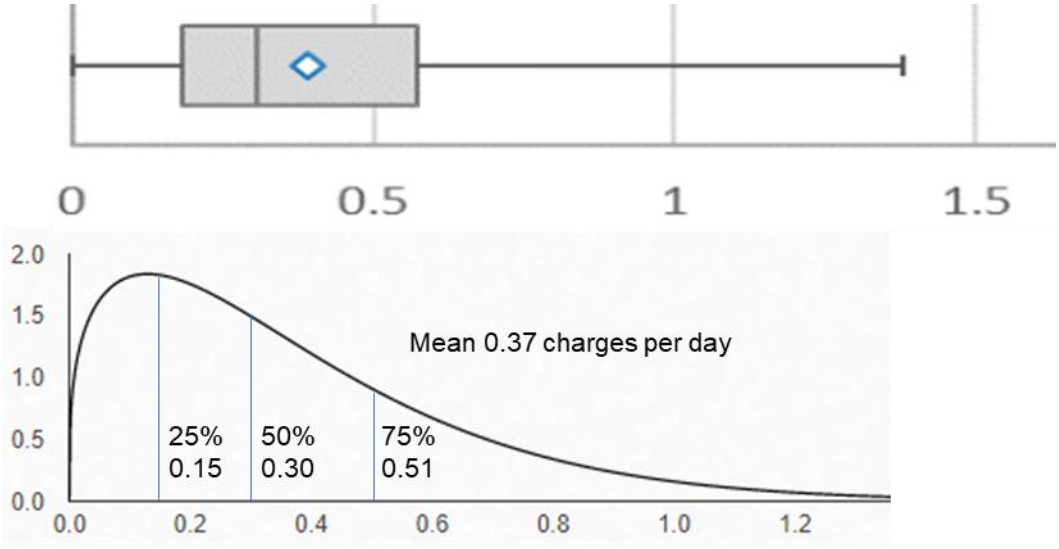

Figure 2: Number of charges per day, [11] Figure 8-7

The resulting distributions, as shown in Figure 1 and Figure 2, have parameters $\alpha = 1.5$, and $\beta = 29$ for charging demand and $\alpha = 1.3$ and $\beta = 0.4$ for the number of charges per day. A customer with, for example, 0.33 charges per day will be modelled as charging every third day.

The idealised parameters are further constrained such that at least one charge occurs per 14 days. The maximum number of charges per day is limited to 1 as the measurement data representing the starting times does not indicate how multiple charging periods should be distributed to avoid overlapping.

The charging energy is sampled independently for each session but the expected number of charges per day is determined once for each customer, representing a consistent behaviour pattern throughout the year. This approach provides a distribution for the mean annual EV charging demand where the mean and quartile values are approximately consistent with the distribution of measured annual demands from the Electric Nation trials as shown in Figure 3.

An alternative approach would have been to randomize both the number of charges and the energy per session for each new day. However, all customers are then equally likely to experience both long and short charges and so all would tend to have the same mean annual demand. Similarly, if the random samples are held constant over the year, then a few customers will have extreme values of both charging frequency and energy per session, giving an unrealistic wide spread of mean annual demands.

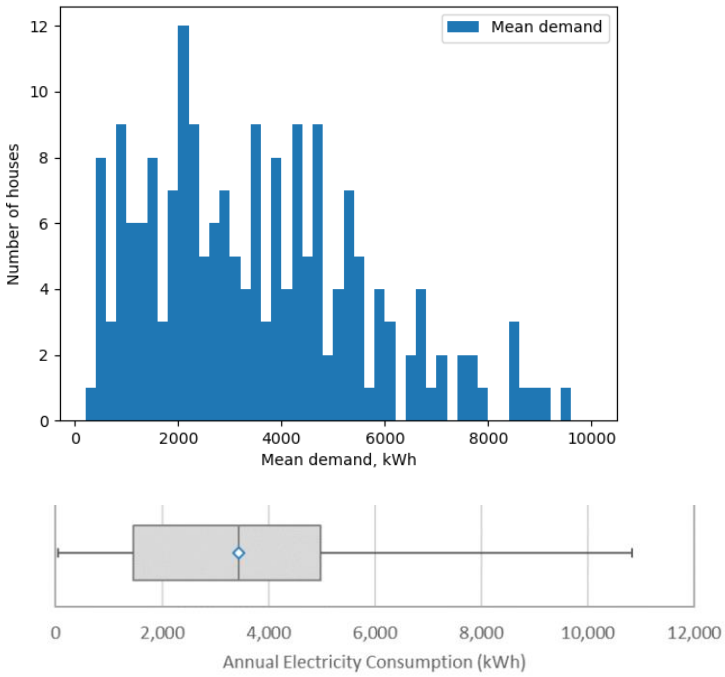

Figure 3: Annual demand for Battery EV charging, 35 kWh batteries, [11] Figure 8-16

The starting time for the charge sessions is also based on empirical data from the Electric Nation trials, represented as a probability density function in Figure 4. This data uses the time that charging actually started, as opposed to the plug-in time, and so allows for any use of timers that the customer may have chosen, though excludes periods within the trial when smart charging was enabled. The data therefore represents the customer preferences without any interventions to manage demand. A starting hour is assigned once for each customer with separate values for weekdays and weekends and with individual daily start-times randomized within the hour.

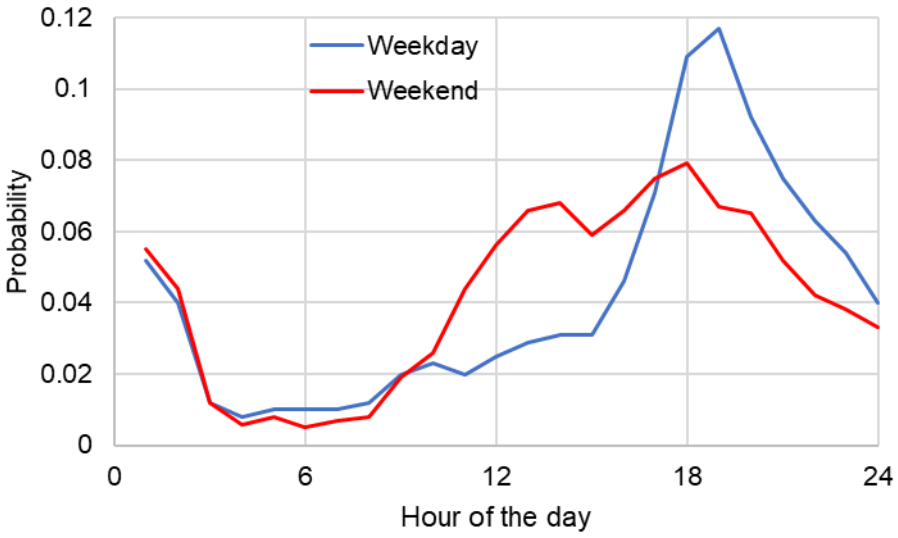

Figure 4: Charging start time, [11] Figure 8-2

A problem can arise with this method where, for example, the weekday charging time is late in the evening, and the weekend charging time is in the early hours of the morning. The model would then include a charging period for the Friday evening, and a weekend charging starting early on the Saturday, possibly before the previous charging had been completed. This occurs relatively rarely,

and so the charging times have been amended such that any new charging session will start after the previous session ends, effectively combining them together.

2.3.6 V2G EV chargers

The V2G mode of operation has been applied to all EV chargers on the LV feeder. The simulation considers a 'worst-case' scenario for exports where each EV exports power for a half-hour period between 1:30 and 2pm, timed to coincide with the expected peak outputs from solar PV and when the demand from EV charging and other appliances is relatively low.

This export profile represents a scenario where V2G exports are called on to provide a grid support service. The assumption that all EVs can participate implies that all the customers on the LV feeder receive the same request to export, and that they all have their EV connected at the appropriate time.

To maximise the likelihood that the simulation will encounter peak voltage deviations, the exports occur each day within the 1-year simulation duration.

Exports use a power of 3.68 kW, as is currently permitted under the G98 regulations. Further work in WP2 will consider higher export powers where this is feasible within the headroom available at each substation. For this initial investigation with completely synthesized demand data, there is a risk that excessively high export power will create unrealistic scenarios.

After the export event has been completed, the EV batteries are re-charged to replace the exported energy. The recharging energy is increased by a factor of 23% $(1/0.81)$ to reflect the combined impact of a 90% discharging efficiency and a 90% recharging efficiency.

Recharging uses the full rated charging power which is assumed to be 7 kW as a worst-case scenario. Since the recharging power is higher than the export power, recharging has a shorter duration. Where the export power is moderated, such as by the volt-watt or volt-var control, the recharging duration is reduced further, rather than the recharging import power. The recharging period is also extended to include any energy that had not been provided if the export event interrupted a period when the vehicle was already charging.

Two options in the model have been considered when modelling the timing of this recharging. Initial models assumed that recharging would take place immediately after the export event.

In a second option, recharging is delayed by a randomised delay of up to 60 minutes. This delay is configured once for each customer and repeated for each export event.

These parameters have been selected on the basis that customers may need to replace the discharged energy as soon as possible, to return to their preferred state-of-charge in the vehicle. An alternative approach could be that customers will delay recharging their batteries until a low-cost tariff period becomes available overnight. If this were the case, they would likely also delay their vehicle charging to an overnight period. Previous work on the Parc Eirin project found that a coordinated behaviour where all customers follow a low-cost tariff would create a new demand peak when this comes into effect, for example at 00:30 if the parameters of the Octopus Go tariff were used in the model. As with the simulations included in this report, some randomisation would still be required to mitigate voltage drops if every customer begins their charging exactly at 00:30.

2.3.7 Volt-watt control

Export powers can be limited by a volt-watt control option. This ramps down the permitted export power based on the customer connection node voltage, as shown in the Control Algorithms report [13].

Initial tests with voltage thresholds based on Australian standard TS129 [14] showed minimal impact on voltage rise. This is to be expected as the settings would mainly inhibit exports for connection voltages that are outside of the permitted margin of 230 V + 10%.

Alternative settings were then adopted such that the maximum exported power would reduce linearly with voltage from 100% of permitted export at 245 V, down to 0% at 250 V.

For reference below, the volt-watt function can be defined to allow a maximum export power $P\_(\max, \mathrm{VW})$ as a function of the voltage

$$P\_(\max, \mathrm{VW}) = f\_\mathrm{VW}\,(V)$$

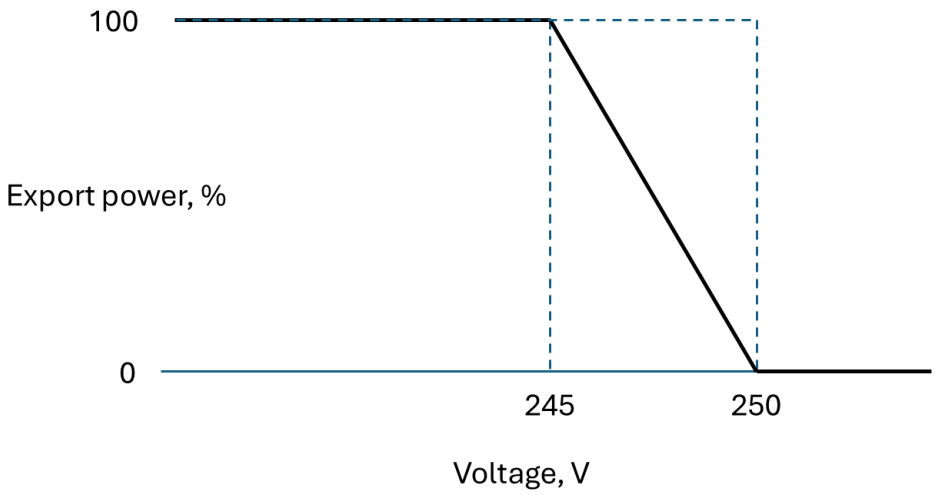

Figure 5: Volt-watt control parameters

2.3.8 Volt-var control

Volt-var control requires reactive power to be imported when the voltage is high and to be exported when is low. Unlike volt-watt control, it therefore addresses voltage drops in addition to voltage rise.

As proposed in TS129 [14], reactive power imports ramp up between 240 V and 258 V to 60% of the rated export power, and exports ramp between 220 V and 207 V to 44% of rated export power.

Where the permitted export power is less than the rated power, it is unclear which should apply when calculating the reactive power. The model assumes that the ratio is applied to the rated power of 7 kW, so giving a greater reactive power contribution than if applied to the export power of 3.68 kW.

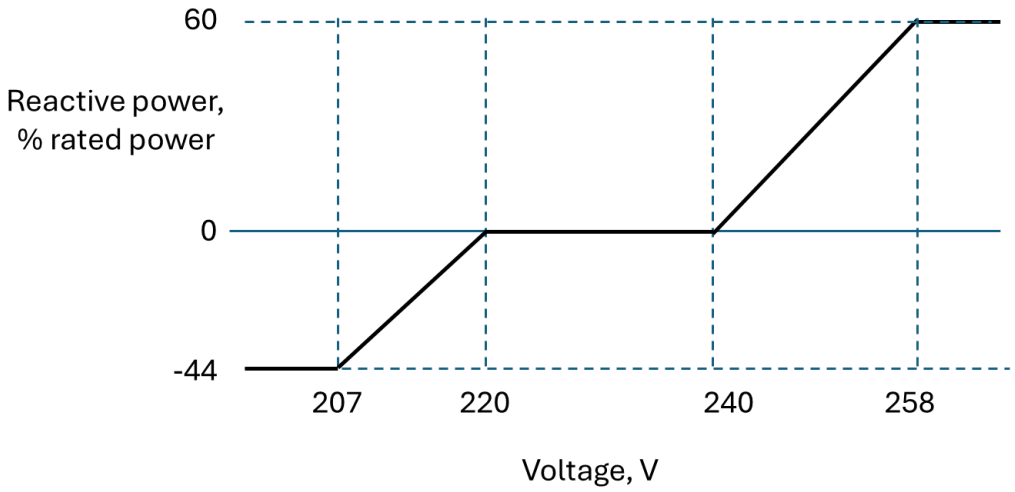

Figure 6: Volt-var control parameters

Volt-var control also has an impact on the maximum active power due to the additional current needed to provide reactive power. The model assumes that the inverter power electronics are limited to an apparent power S of 7 kVA, such that the full 7 kW active power can only be achieved at a power factor of unity. Any reactive power reduces the maximum active power $P\_(\max, \mathrm{VV})$, such that

$$P\_(\max, \mathrm{VV}) = \sqrt{(S\text{^}2 - Q)}$$

where Q is the reactive power, defined by the volt-var control function f_VV so that $Q = f\_\mathrm{VV}\,(V)$.

2.3.9 Application of volt-watt and volt-var control

Both volt-watt and volt-var control functions have the potential for instability since the active power varies according to the voltage, but any change in the active or reactive power will then affect the voltage.

Similarly, where there are multiple controlled inverters on the LV feeder, if one inverter reduces power in response to a voltage rise, the voltage at a second inverter will then also reduce, enabling the second inverter to increase power.

These interaction effects will be covered later in the project in WP3 and so the modelling approach bases the control function on the time-series voltages that were observed in a separate simulation where the control technique was not applied. This potentially overestimates the impact that could be achieved, but will also tend to constrain exports to a greater extent. In effect, if there was a high voltage rise without the control technique, and if this is experienced by multiple EV chargers, they will all respond. However, it may have been sufficient for only some of the EV chargers to respond to the control function, and this might lower the voltage for other EV chargers such that they were not constrained. For this initial investigation, the modelling approach shows the maximum mitigation to voltage rise that might be achieved, accepting that some EV chargers may be constrained more than necessary.

The simulations use the following steps:

- The model volt-var control, if this is selected, and calculates the reactive power Q that should be imported or exported for each sample, based on the voltage time-series for a separate simulation without volt-var control.
- Once the reactive power has been defined, the maximum active power $P\_\max$ can be calculated, as above. This maximum active power applies to both import and export, such that for any sample $|P| \leq P\_(\max, \mathrm{VV})$.
- The total delivered EV charging energy is calculated and the charging start time.
- For each sample within the charging period, the charger operates at the minimum of the rated power or the maximum active power. Charging continues on successive samples until the required charge energy has been delivered.
- A similar process applies to exports, but with a defined end-time rather than a defined energy delivery.
- For each sample within the discharging period, the charger operates at the minimum of the permitted export power, the maximum active power $P\_(\max, \mathrm{VV})$ allowing for the reactive power, and if volt-watt control is active, the maximum active power for export $P\_(\max, \mathrm{VW})$.

2.4 Simulation configuration

The simulation covers a 1-year period at 1-minute resolution.

Results are generated independently for each LV feeder and for each substation, then aggregated to present overall trends.

The voltage at the substation is assumed to be a constant 245 V on each phase and so variations due to tap changes are not included.

Results are presented based on the following metrics:

Maximum customer voltage	Calculated for each LV feeder at 1-minute resolution at each single-phase customer connection, taking maximum over time and over three phases.
Minimum customer voltage	Calculated for each LV feeder at 1-minute resolution at each single-phase customer connection, taking minimum over time and over three phases.
Mean cable losses	Averaged for each LV feeder over the one-year simulation period at 1-minute resolution.
Maximum RMS first branch current	Maximum for each LV feeder over the three-phases of the RMS current in the first cable branch from the substation on each feeder, averaged over the one-year simulation period at 1-minute resolution. The first branch typically provides the most significant current constraint as it carries the aggregated demand for all customers on the feeder.
Current overloads	Numbers of mains branches for each feeder using the peak current from a half-hourly daily profile, calculated according to the Elexon seasons, for each cable branch and over the three phases.

It may be useful to note that the maximum and minimum voltages capture extreme events. It is possible that either of the control methods may have a benefit by reducing the frequency at which high voltages occur, even if the maximum over all time samples remains the same.

The mean loss and RMS substation current are averaged over the full duration of the simulation and so these metrics do reflect benefits of a reduced frequency of peaks, as well as depending on the extreme events. However, results presented here showing mean losses depend on the frequency with which V2G export events occur. This has arbitrarily been set here to be daily, such that there is a greater change of identifying peaks due to extreme conditions. Interpretation of any reductions in mean losses would therefore need to bear in mind that the benefit may be negligible if the export events happen very rarely.

3. Results for sample substation 892320

This section presents results for one specific substation, selected for a more detailed investigation as the initial results for V2G with volt-watt control showed an increase in voltage deviations, rather than the intuitively expected decrease. Results here use the initial impedances based on WinDEBUT, and a default EAC rather than the actual EAC as recorded in CROWN. Maximum and minimum voltages are calculated here over all three phases, although in practice only the voltage at the connected single-phase would need to be considered.

3.1 Volt-watt control

Figure 7 shows the total active powers, aggregated over all customers and phases, for one export event. This is the total power delivered to customers, including the power to the EV chargers. During the export event the total power is negative, followed by a recharging period immediately after. Without volt-watt control, the recharging has a shorter duration than the export period since recharging operates at 7 kW and exporting only at 3.68 kW. The recharging period appears as a step in demand, just as with the export period, because the model assumes that all customers have exported the same energy, and that recharging starts at the same time.

The plot also shows operation with the volt-watt control. The export power is significantly reduced, with the reduction being roughly constant across the export period. Some customers were unable to export at all, so the spike in recharging power has a reduced peak. The recharging duration also reduces with a gradient, rather than as a step, because the exported energy now differs between customers, and some require less time to recharge.

Figure 8 shows the maximum and minimum voltages, looking over all LV feeders, phases and time-samples. The voltage rise effect has been successfully mitigated by volt-watt control during the export period, but there are worsened voltage deviations at the start of the recharging period.

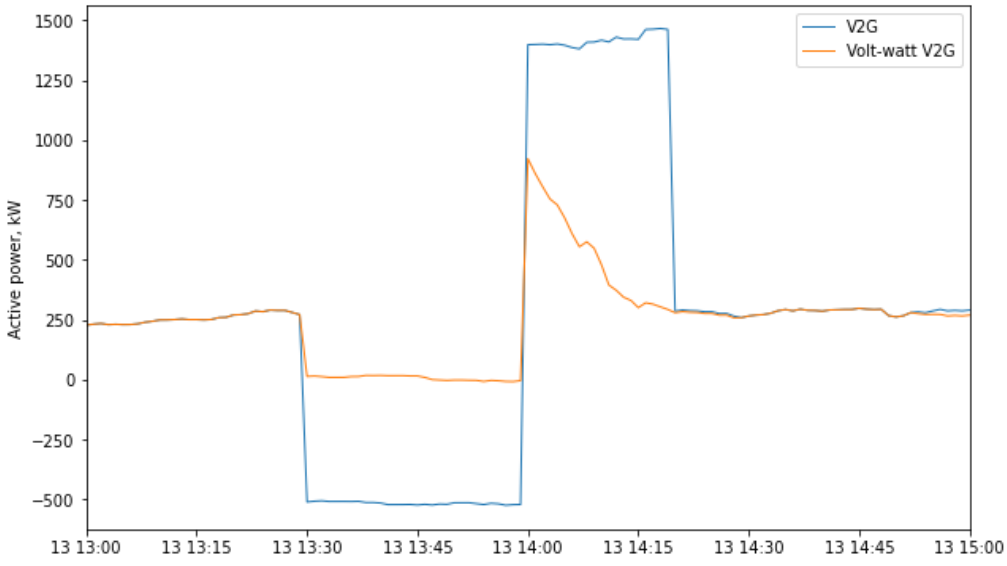

Figure 7: Substation 892320, volt-watt control, export event active powers

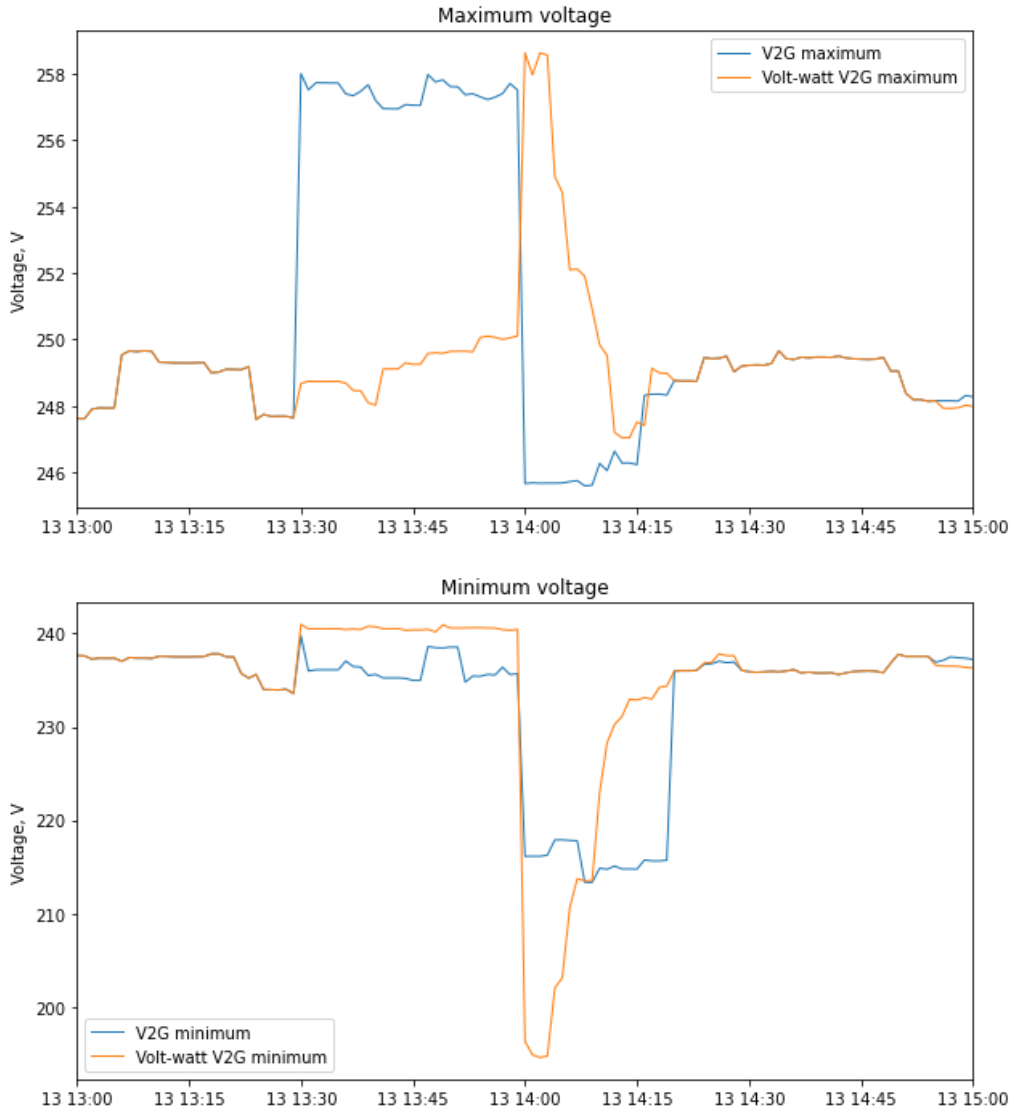

Figure 8: Substation 892320, volt-watt control, maximum and minimum voltages

The worst-case dip to 194 V occurs at one particular MPAN **[reference removed]** on phase L3, as shown in the following plots. Figure 9 shows the active power, with a reduced power in the export period due to volt-watt control and a reduced duration of recharging afterwards. Figure 10 shows the voltages at this particular MPAN.

In this particular instance, most of the customers on phases L1 and L3 are prevented from exporting by the volt-watt control and the voltage is above 250 V for most of the route to **MPAN [reference removed]**. The voltage on L3 is lower, partly as there are fewer chargers, and also because the greater exports on phases L1 and L2 cause the voltage on L3 to fall. The customers on phase L3 mostly continue to export when volt-watt control is applied and so their recharging demand remains the same, whereas there is minimal recharging for the customers on L1 and L2.

In the recharging phase, the import power on L3 with volt-watt control is similar to that with no control. whereas the import power on phases L1 and L2 is much lower. This unbalance causes voltage rise on phases L1 and L2, which in this case creates a greater peak than would have occurred in the more balanced export period without volt-watt control. The voltage drop on phase L3 is worsened as the model assumes a constant power mode of operation, such that the current is further increased if the voltage is reduced, leading to the very low voltage shown in Figure 10.

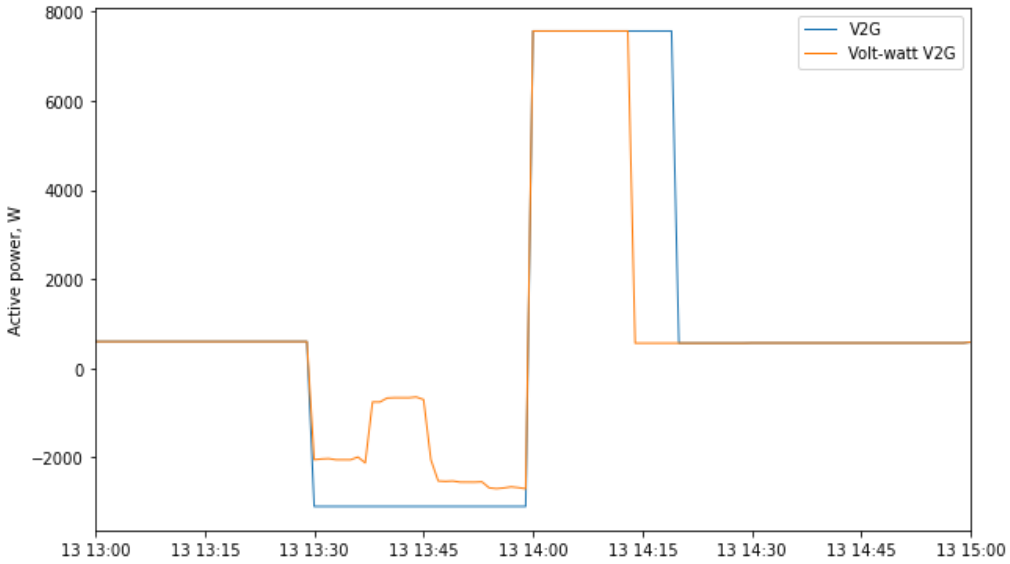

Figure 9: Customer **[reference removed]**, volt-watt control, export event active powers

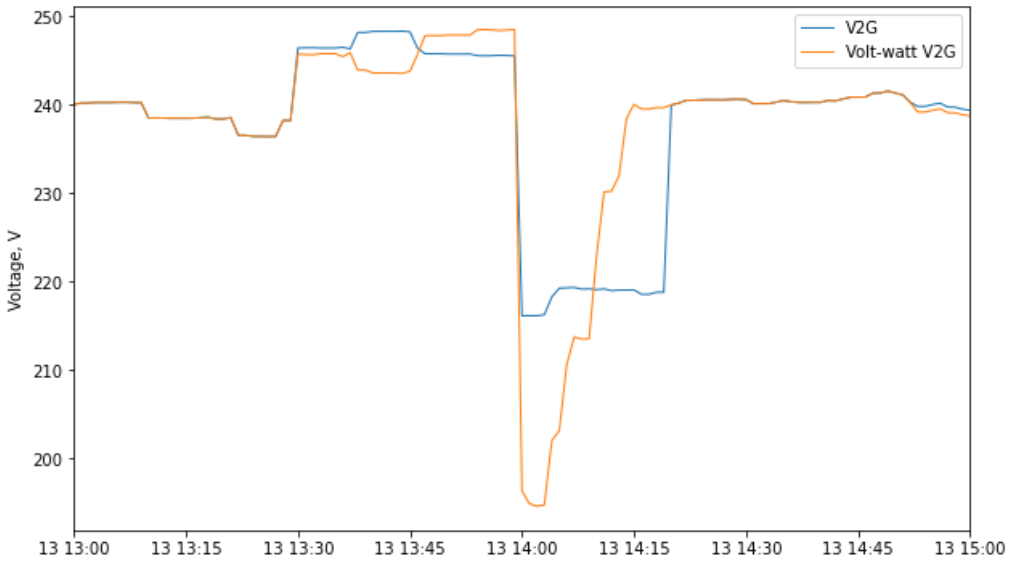

Figure 10: Customer **[reference removed]**, volt-watt control voltages

3.2 Volt-watt control with diversified recharging

The problems caused by coordinated recharging after an export event can be avoided by applying a randomised time delay to each EV charger. This has been modelled by adding a random delay of between 0 and 59 minutes to the start of the recharging period. Figure 11 shows the maximum and minimum voltages for this case and demonstrates that the impact of the recharging period is much reduced. Maximum voltages are reduced with volt-watt control, as are the minimums during the recharging period.

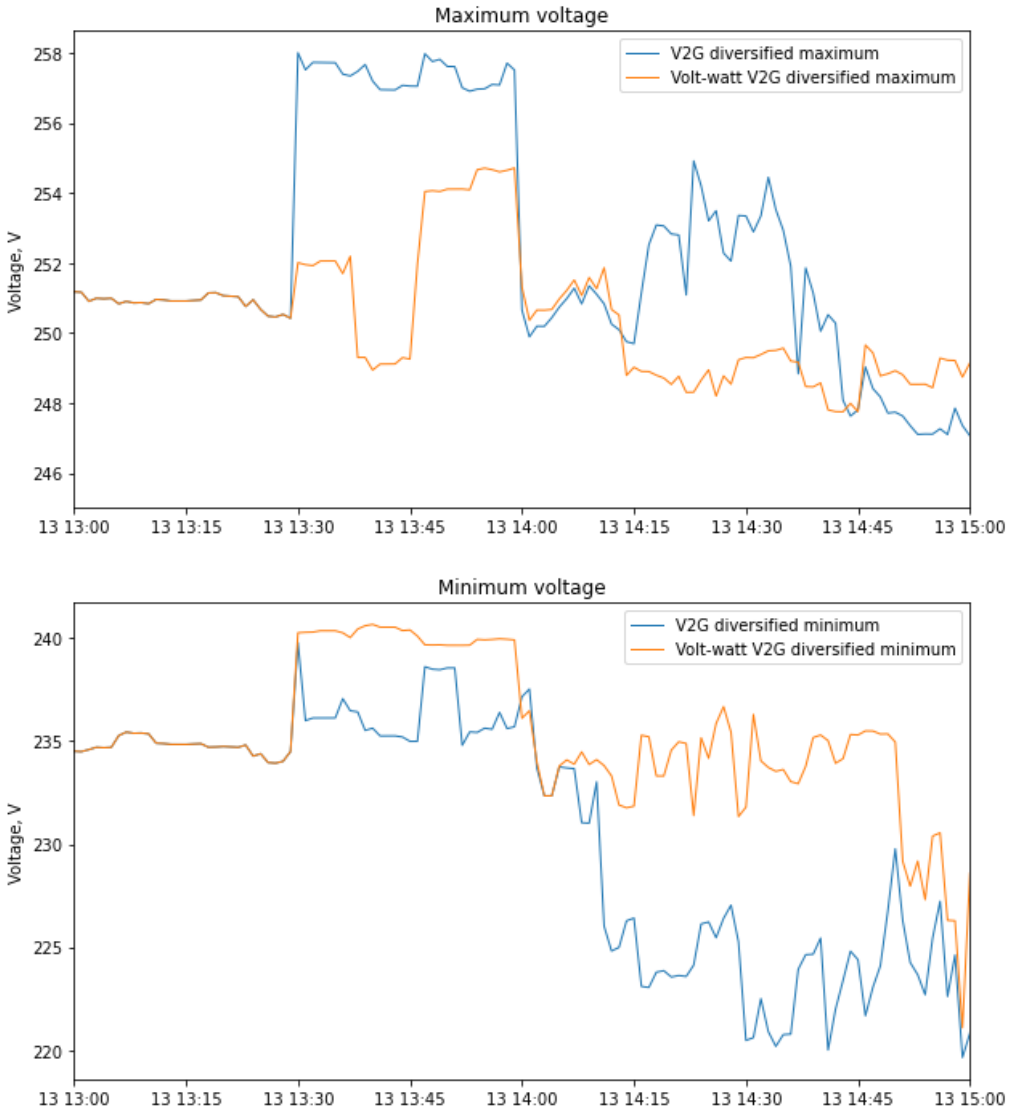

Figure 11: Substation 892320, volt-watt control with diversified recharging, maximum and minimum voltages

3.3 Volt-var control

The same export event is now investigated where volt-var control is applied. This makes no material difference in this case to the active powers, which are as above for the V2G model in Figure 7. During the export event, voltage on phase L1 and L2 are high so volt-var control consumes reactive power, as shown in Figure 12. In this case the voltages in the recharging period as not so low that reactive power needs to be generated, but reactive power is consumed to some extent at all times, as the simulation assumes a busbar voltage of 245 V.

Figure 13 shows the corresponding voltages. For some time-samples during the export period there is a reduction in voltage rise due to the volt-var control, but at other times the voltage is higher. This could be explained by an increased unbalance on the feeder, as most of the reactive power consumption will occur on phases L1 and L2 where voltages are higher, pulling down the voltage on those phases but with a corresponding rise on phase L3.

There may be a further impact in the model of the constant power load behaviour, such that the control to reduce voltage then requires a greater current for the same power to be exported, creating further voltage rise that opposes the control method. This constant power behaviour applies to all loads on the network, not just the EV chargers.

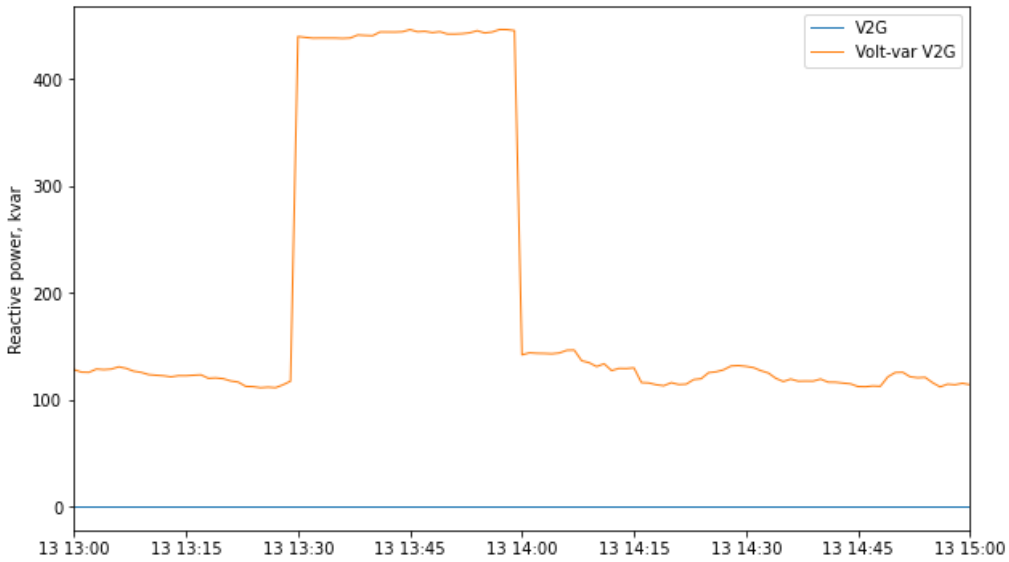

Figure 12: Substation 892320, volt-var control, export event reactive powers

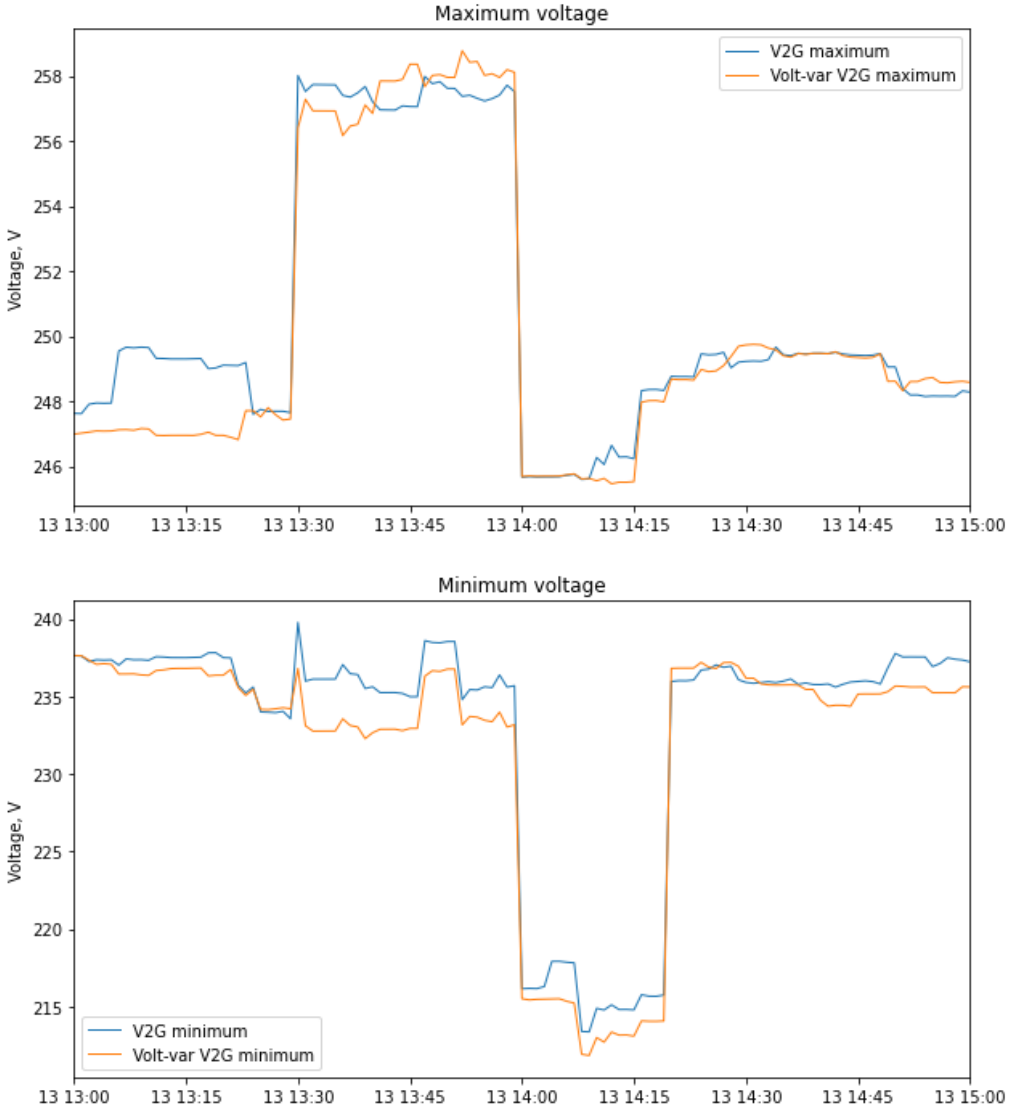

Figure 13: Substation 892320, volt-var control, maximum and minimum voltages

4. Results for selected substations

The results here use the revised impedance data based on SD5H [2], and existing demand data based on EAC records from CROWN. Maximum and minimum voltages are calculated for only the connected phases at each customer meter point.

Results for each scenario are presented first as a series of histograms. These are then summarised in the following section with results for all scenarios plotted together as cumulative distribution functions.

4.1 Baseline

The baseline model has no LCTs and uses a demand model based only on Elexon profiles. Results for the baseline model are aimed at demonstrating that the selected LV feeders are likely to be within capacity bounds initially, before the addition of any further LCTs.

Some customers may already have LCTs, in which case the impact of these will be reflected in the customer EACs but not taken into account in the daily demand profiles which still assumes the Elexon half-hourly mean values based on conventional appliances.

There are no feeder main branches in the results that are flagged as having overloaded RMS currents.

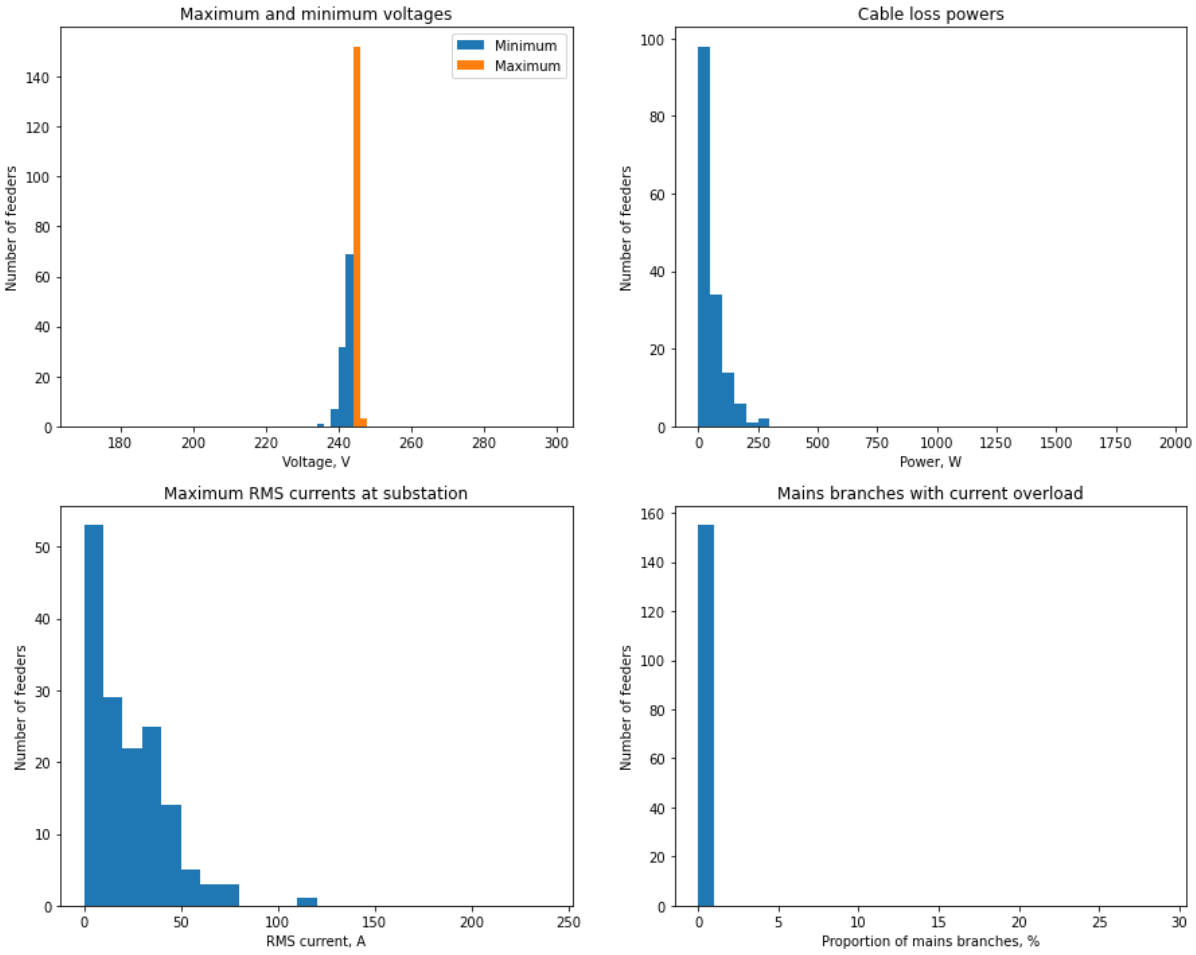

Figure 14: Summary results, baseline

4.2 Added LCTs

Where solar PV, heat pumps and EV chargers are added, maximum and minimum voltages deviate much further from the nominal 245 V assumed at the substation busbar. In practice, many feeders would require some form of intervention to bring their operation back within capacity limits, or the numbers of LCTs would need to be reduced. However, the examples still provide a useful indication of the unconstrained impact of LCTs and the intention here is to assess how the control techniques mitigate these effects.

The peak range of RMS currents at the substation is roughly doubled when the LCTs are added, and there is a corresponding increase in the LV cable losses. However, for the models considered so far, all the feeders remain within the selected current limits.

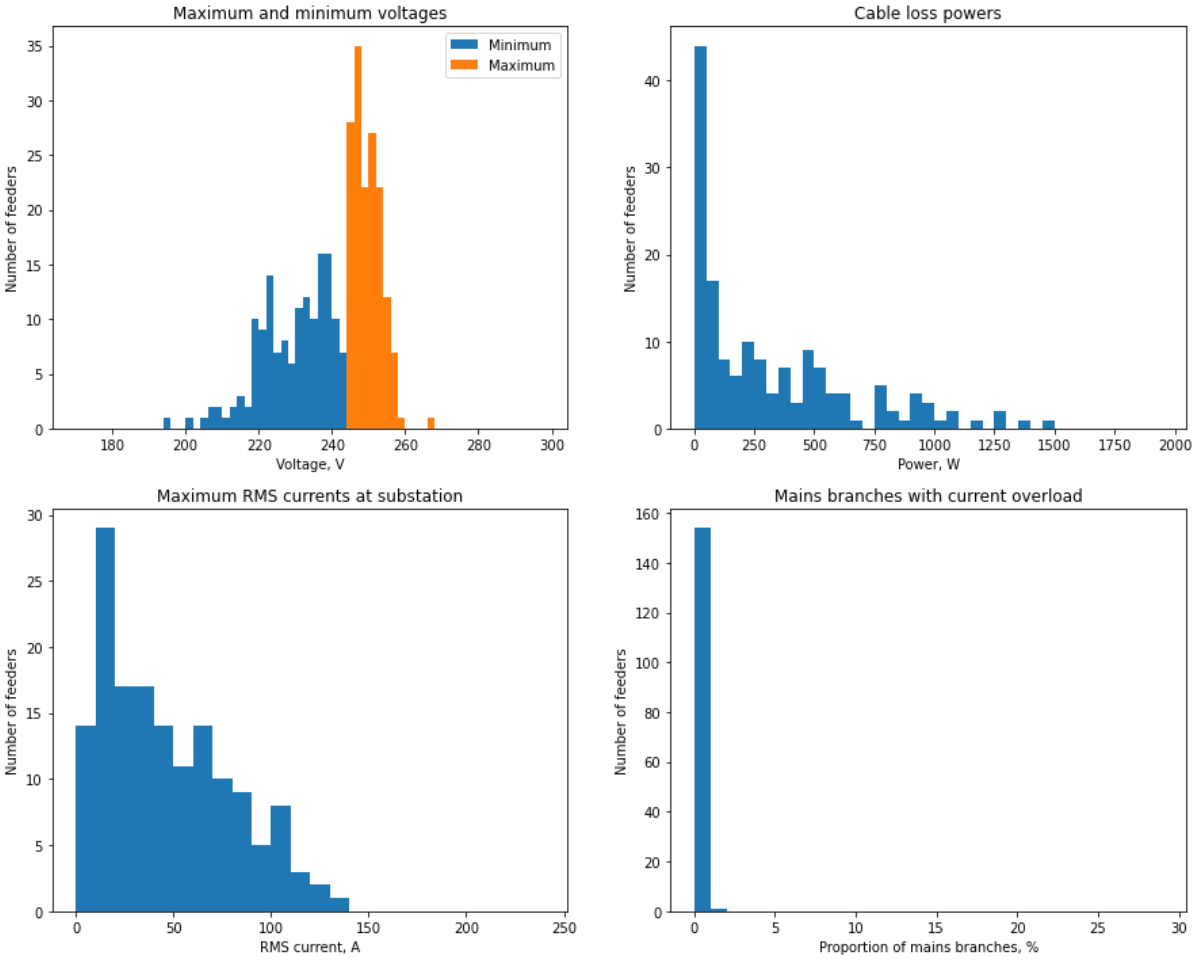

Figure 15: Summary results, added LCTs

4.3 V2G

When the V2G exports are included, there is a further increase in the worst-case voltage deviations, both as voltage rise during export and voltage drop during the subsequent recharging. Losses and peak current are also increased.

For this model, the number of feeders with current overloads has also increased and some of the substations now have branches exceed their rated capacities.

As a caveat to this, a model of a feeder main with many junctions will have many individual branches, whereas a long feeder may just have one branch that covers a long distance. The indicated number of branches exceeding limits will appear much higher where there are many short sections that are counted individually.

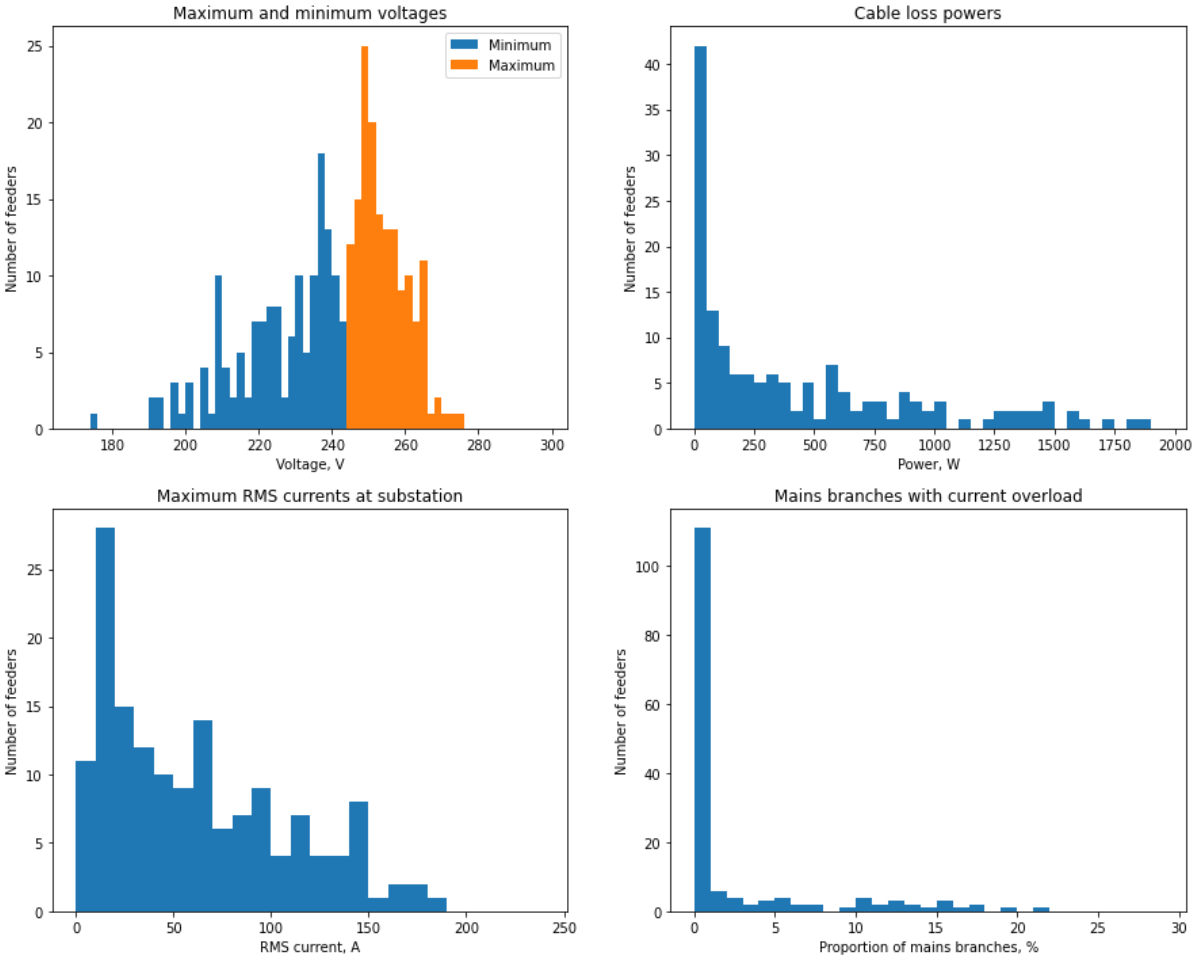

Figure 16: Summary results, V2G

4.4 Volt-watt V2G

In the results presented here with volt-watt control, recharging occurs immediately after the V2G export periods. As shown in the example for substation 892320 above, volt-watt control in this model does not necessarily lead to improved voltage ranges and in the worst-case voltage rise and drops can increase. This effect is seen here where there are more extreme voltage drops, and an approximately similar distribution of voltage rises. However, the worst-case voltage rise is for some feeders and the histogram shows increased clustering around the centre in addition to a greater spread of extreme values.

However, all of the thermal effects are improved compared to V2G, with reduced losses, aggregated RMS currents and number of current overloads.

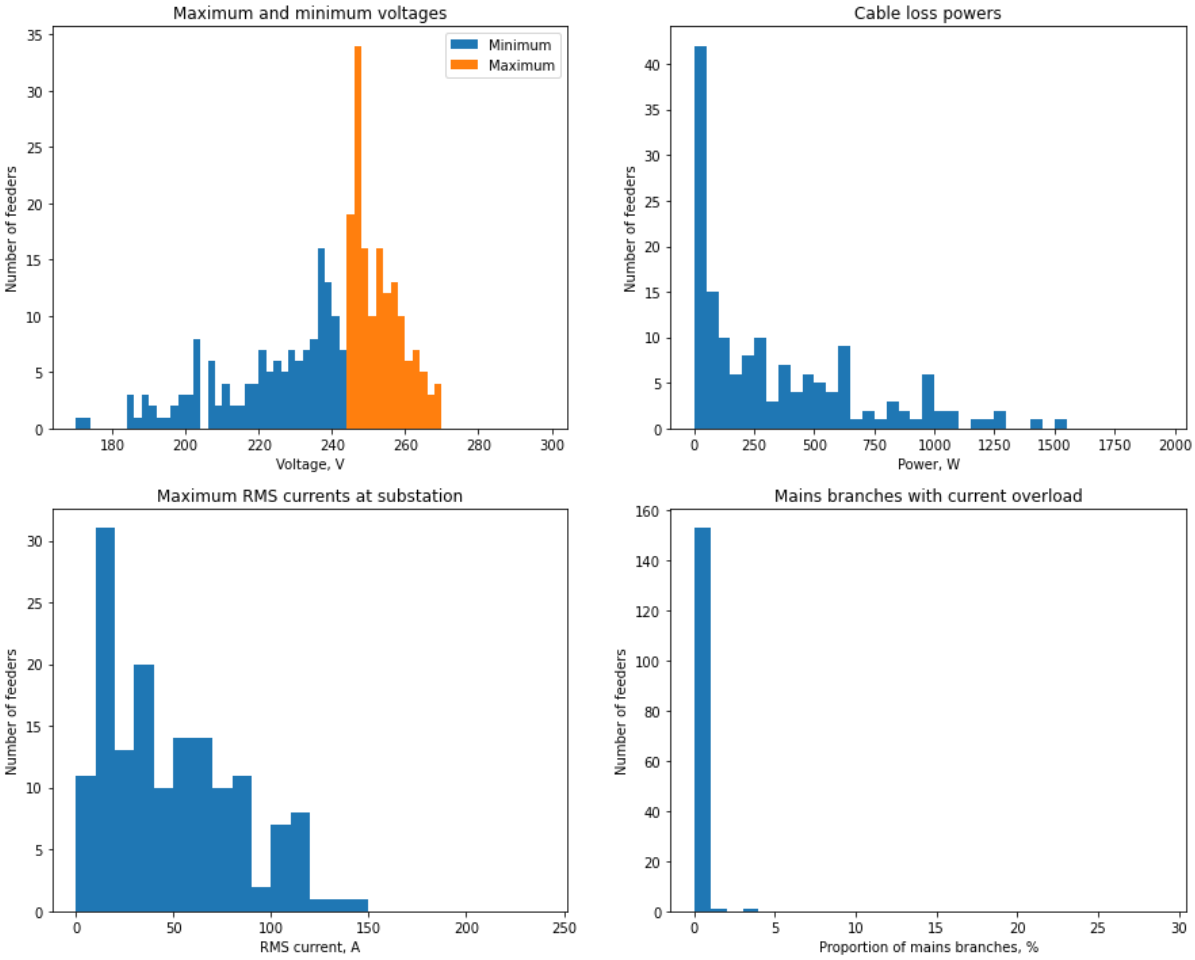

Figure 17: Summary results, volt-watt V2G

4.5 Volt-var V2G

The results here for volt-var control with recharging immediately after the export period show some benefit relative to V2G with no control, although the improvement appears less than with the volt-watt control.

As would be expected where amplitudes are increased by reactive power, the RMS substation currents and mean losses are both increased by the volt-var control. However, the number of current overloads is similar to the case without volt-var control.

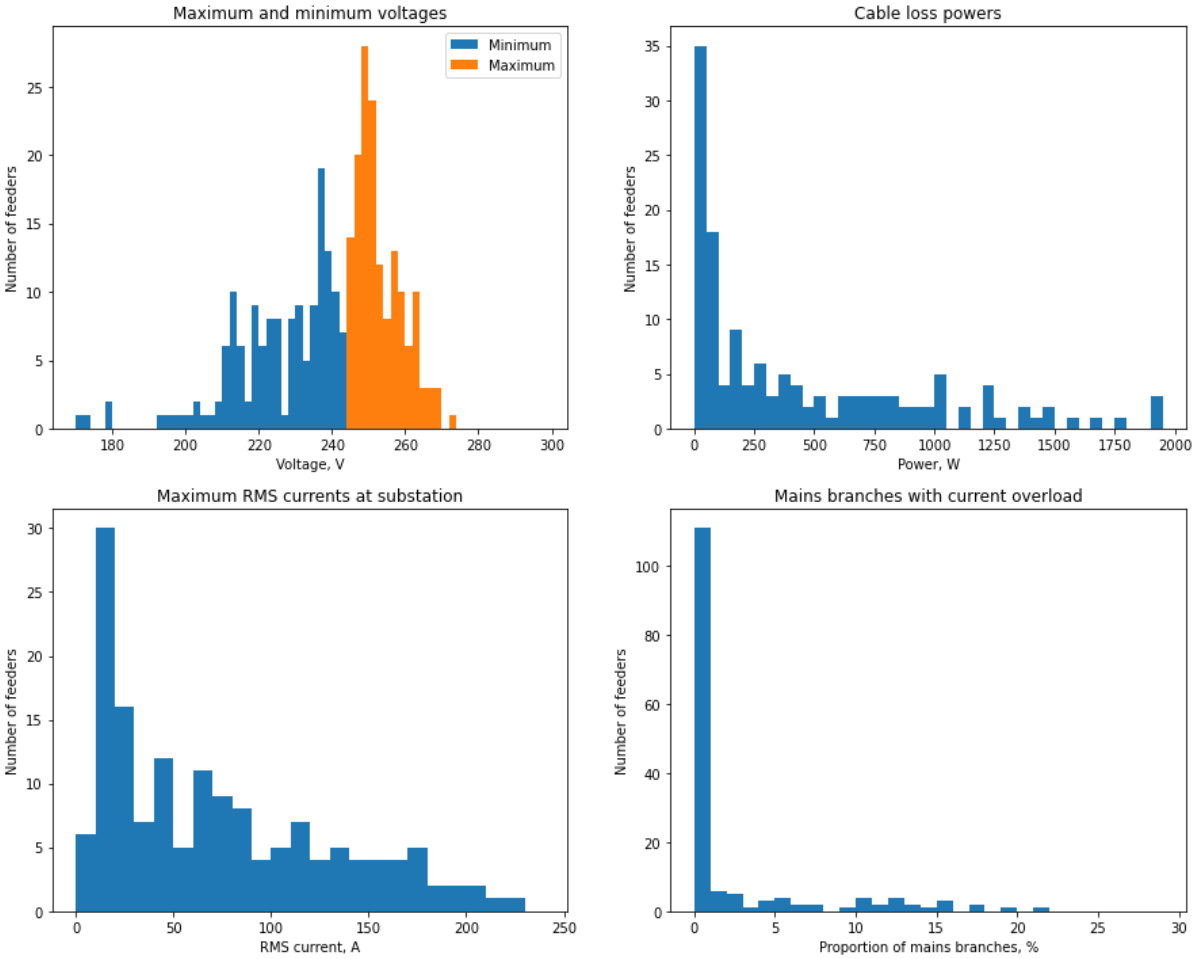

Figure 18: Summary results, volt-var V2G

4.6 V2G with diversified recharging

The results here show the impact of adding a randomised time delay to the recharging that occurs after V2G exports. No other control techniques are applied. Diversifying time recharging behaviour slightly reduces the maximum and minimum voltages, and also gives a reduction in the maximum aggregated currents at the substation. There is a corresponding slight reduction in cable losses.

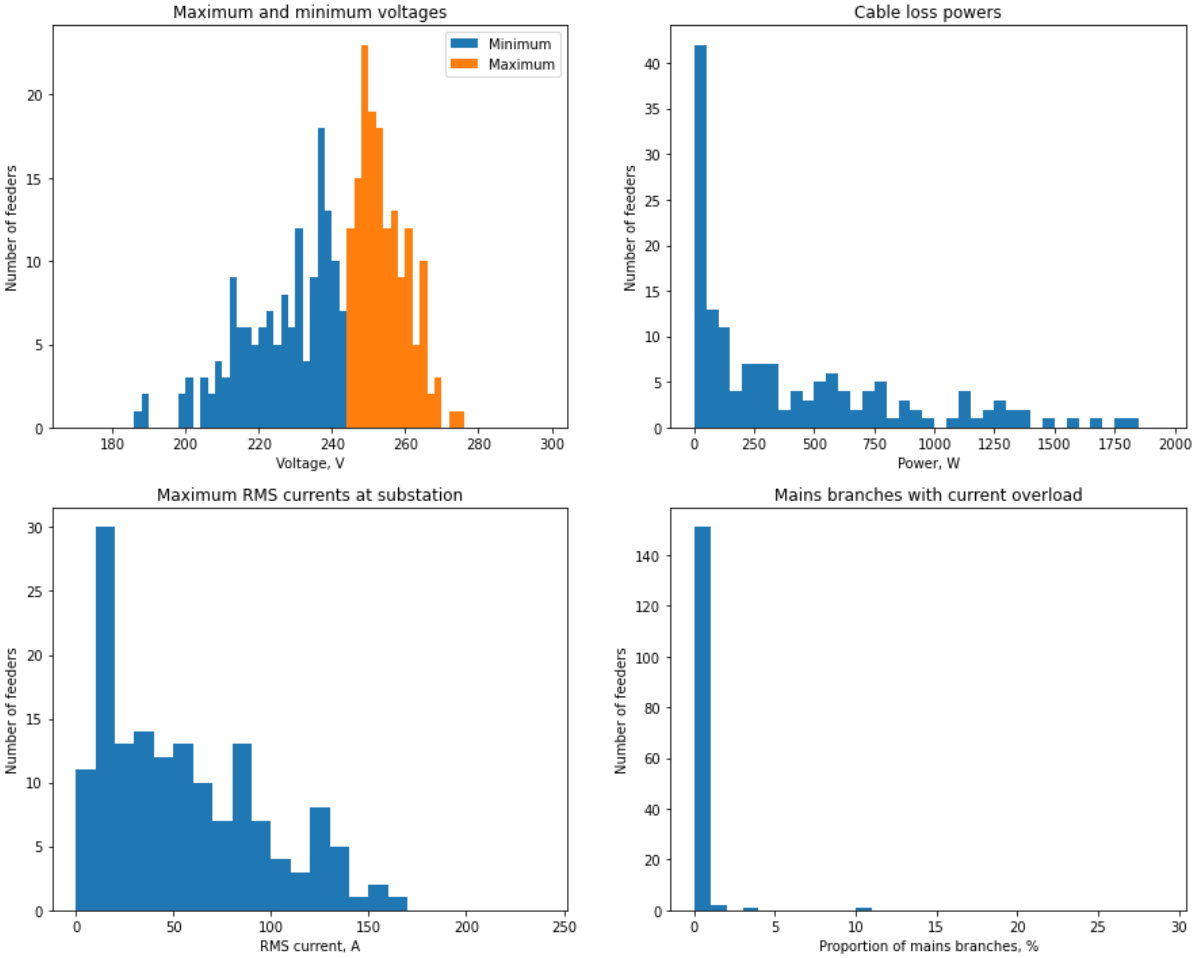

Figure 19: Summary results, V2G with diversified recharging

4.7 Volt-watt V2G with diversified recharging

Diversified recharging avoids the increase in voltage drops noted above for volt-watt control. There is minimal impact on the voltage rise. There is a clear benefit relative to volt-watt control with synchronised recharging, with extremes due to voltage rise and voltage drops both being reduced. Since the randomised delay only affects the recharging period, this again suggests that some of the maximum voltages observed are due to phase unbalance during the recharge period rather than being directly due to high export powers.

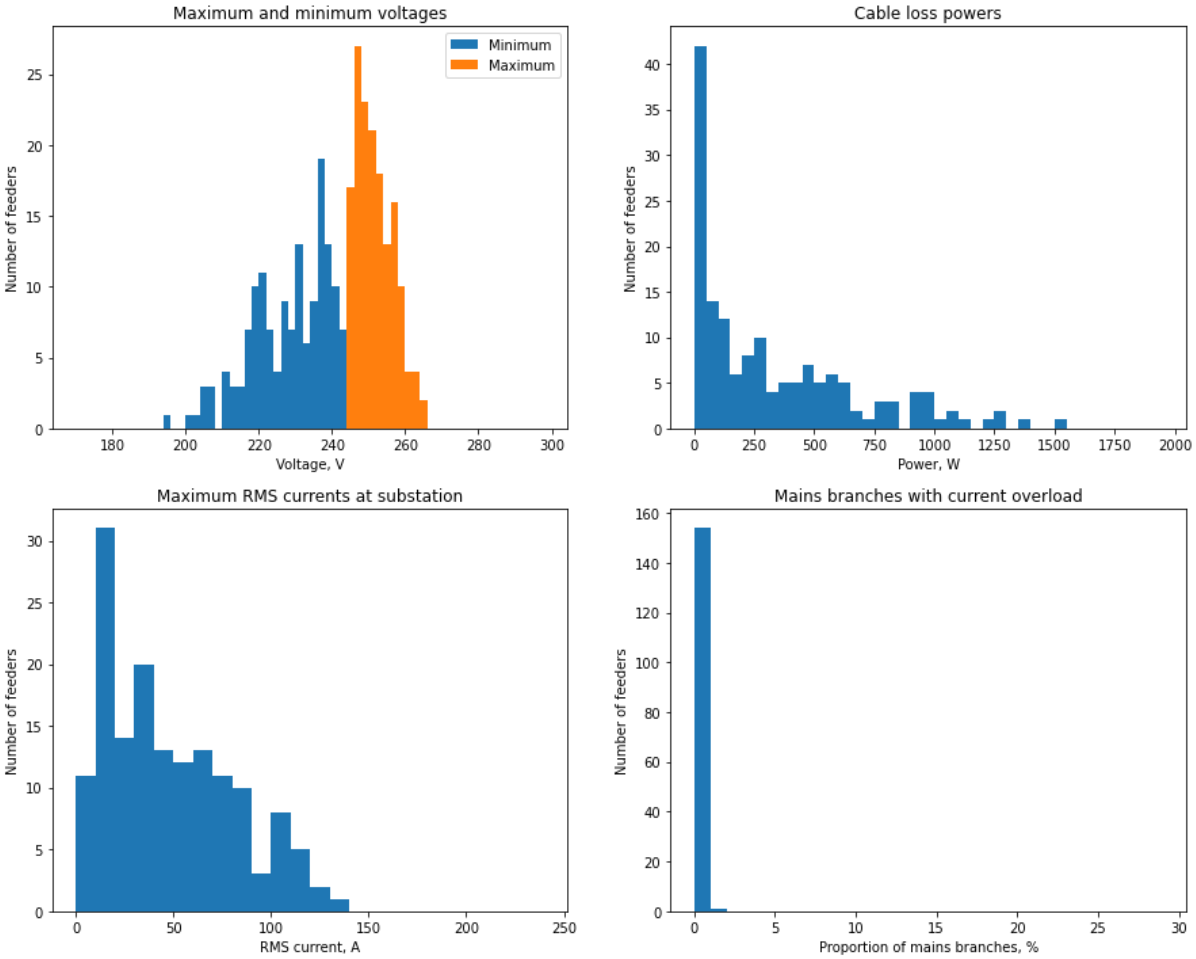

Figure 20: Summary results, volt-watt V2G with diversified recharging

4.8 Volt-var V2G with diversified recharging

Relative to V2G with diversified recharging, there is a similar impact from volt-var control as for V2G with synchronised recharging. RMS substation currents and mean losses are increased, but the maximum and minimum voltage ranges and the number of current overloads remains similar.

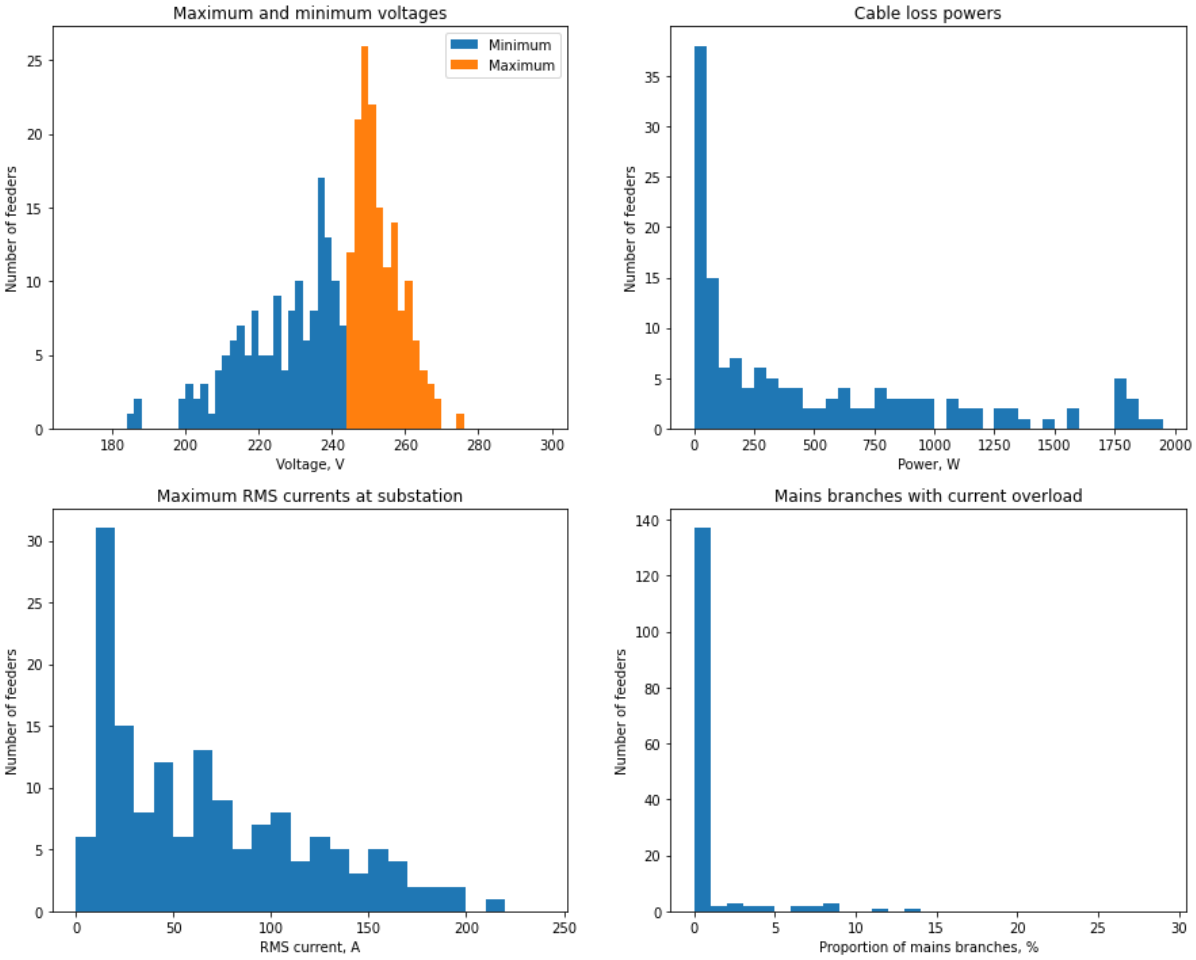

Figure 21: Summary results, volt-var V2G with diversified recharging

5. Summary results

This section presents the same results as in the section 4 but in the format of cumulative distribution functions. These could be less easy to interpret than the histograms shown above but they allow the trends for multiple scenarios to be compared more easily.

Taking Figure 22 for example, this shows that all of the baseline scenario results had a maximum customer voltage less than 245 V, but there were outlier voltages the V2G scenario up to 274 V. The improvement due to control methods can be quantified, for example, by noting that 75% of feeders for the V2G scenario had a voltage at or below 253 V, but with volt-watt or volt-var control, approximately 80% of feeders where below this same threshold.

5.1 Maximum voltage

The summary results below in Figure 22 show volt-watt control reducing the worst-case voltage rise by around 15 V, and volt-var control providing a reduction of only around 5 V.

Results in Figure 23 with diversified recharging are similar, as expected since the diversification process does not affect the export period.

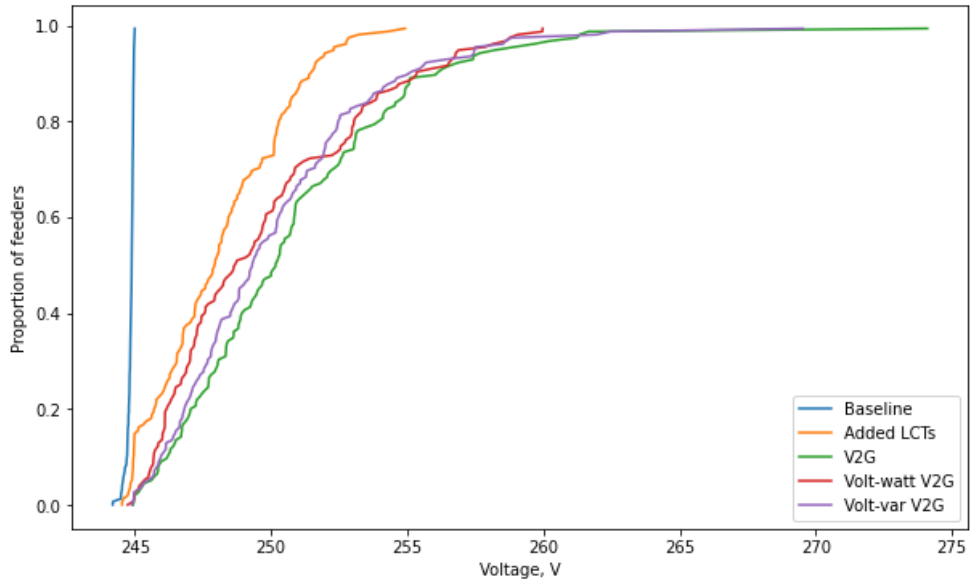

Figure 22: Maximum voltage at customer meters per feeder, without diversified recharging

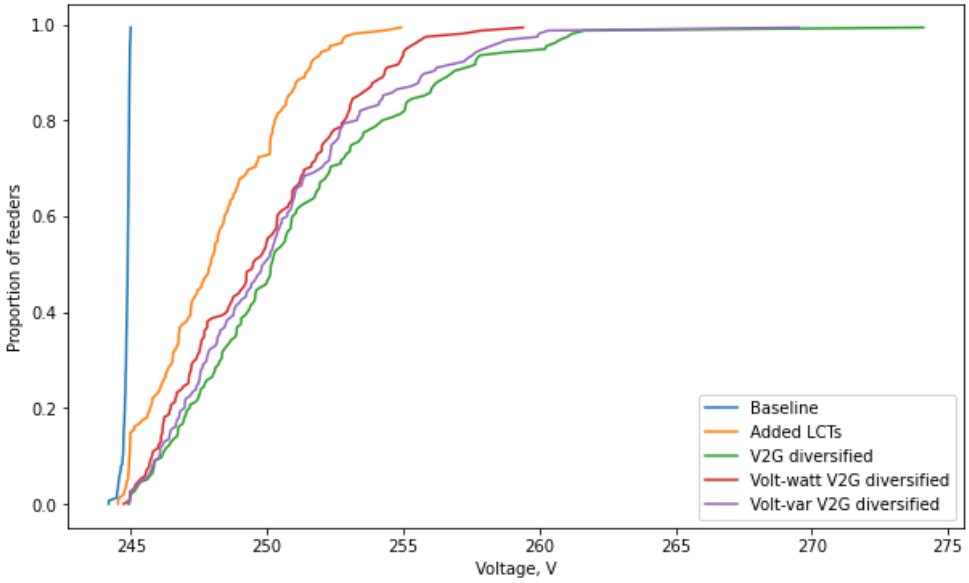

Figure 23: Maximum voltage at customer meters per feeder, with diversified recharging

5.2 Minimum voltage

Figure 24 shows the worst-case voltage drops, which are worsened by around 5 V with volt-watt control and less so by volt-var control. This effect appears to be due to the asymmetrical impact of the control methods where customers on one phase with high voltages will have most reduction applied to their export powers. In the algorithm used here, recharging still happens simultaneously and voltage drops are greater where the imported power is more unbalanced.

Diversified recharging as in Figure 25 avoids the very high voltage drops associated with simultaneous imports after the export period has ended. Although volt-var control includes reactive power export when voltages are low, the worst-case voltage drops are still lower than without the control techniques.

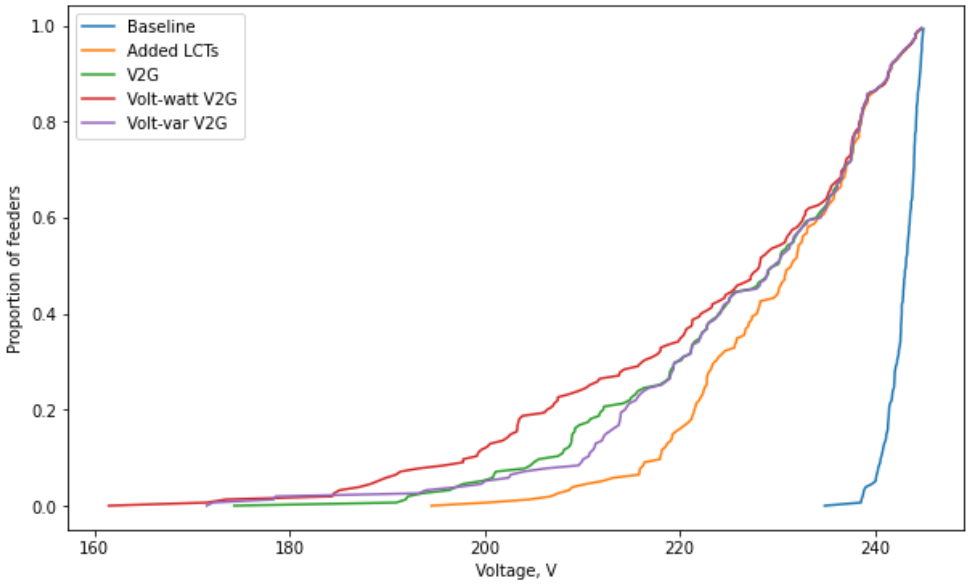

Figure 24: Minimum voltage at customer meters per feeder, without diversified recharging

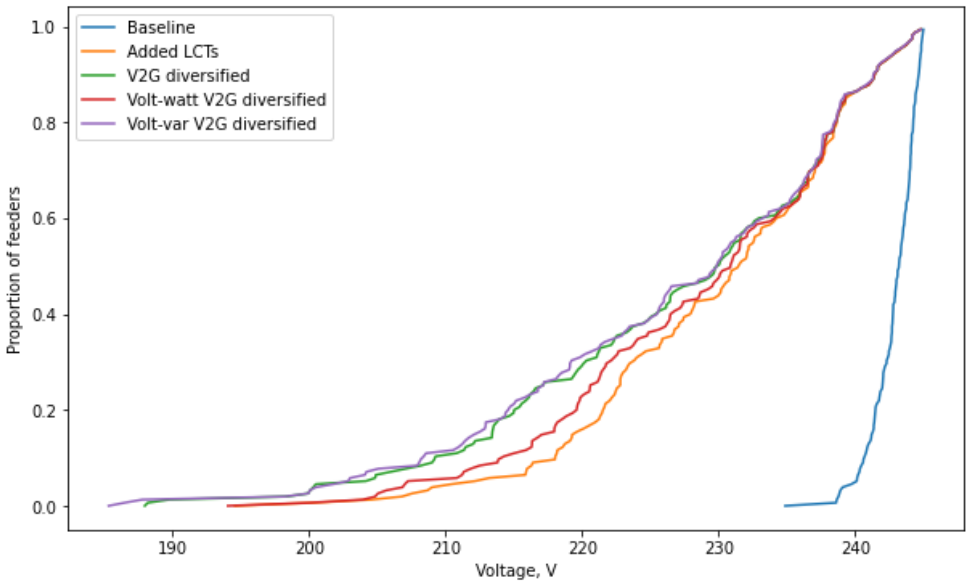

Figure 25: Minimum voltage at customer meters per feeder, with diversified recharging

5.3 Cable loss powers

Figure 26 shows the cable loss powers, where the increase due to V2G is effectively mitigated by the volt-watt control. However, this also indicates that the benefit from V2G exports has also significantly reduced with the volt-watt control. Conversely, losses with the volt-var control are increased due to the increased current amplitude caused by the additional reactive power.

The loss powers are similar regardless of the time profile of the recharging, with losses being spread over a longer period rather than just at the peak when recharging would otherwise be more synchronised.

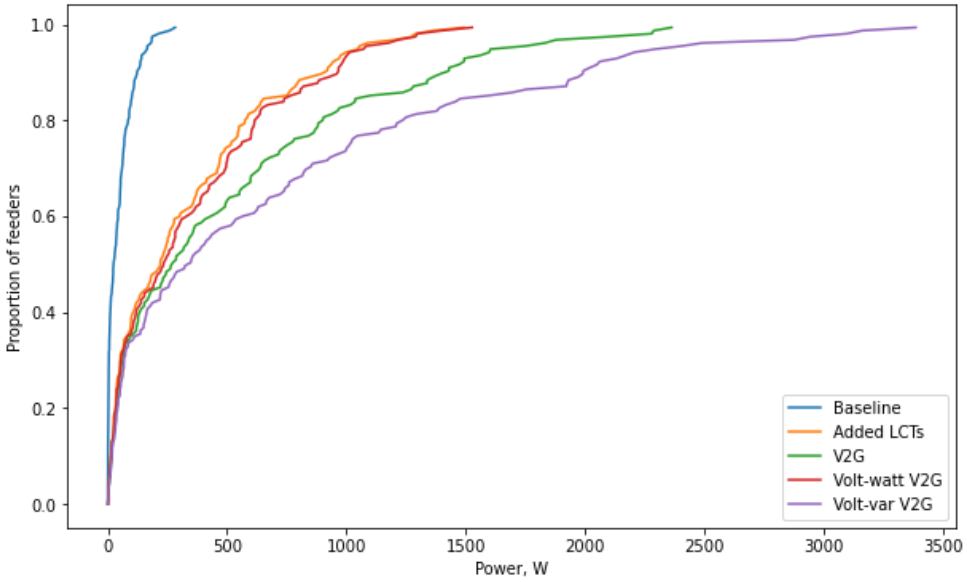

Figure 26: Cable loss powers per feeder, without diversified recharging

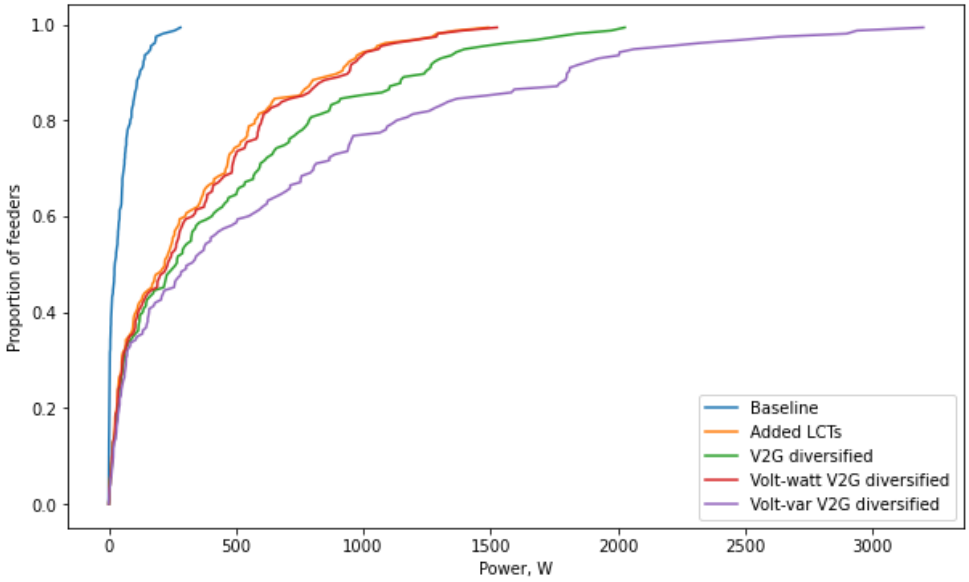

Figure 27: Cable loss powers per feeder, with diversified recharging

5.4 Maximum RMS currents per feeder

Figure 28 shows the distribution of maximum RMS currents per feeder, for the aggregated current at the substation. With volt-watt control this is only slightly higher than without the V2G function, suggesting that a large proportion of the exports have been blocked by the control action. As with the losses, currents are higher with the volt-var control.

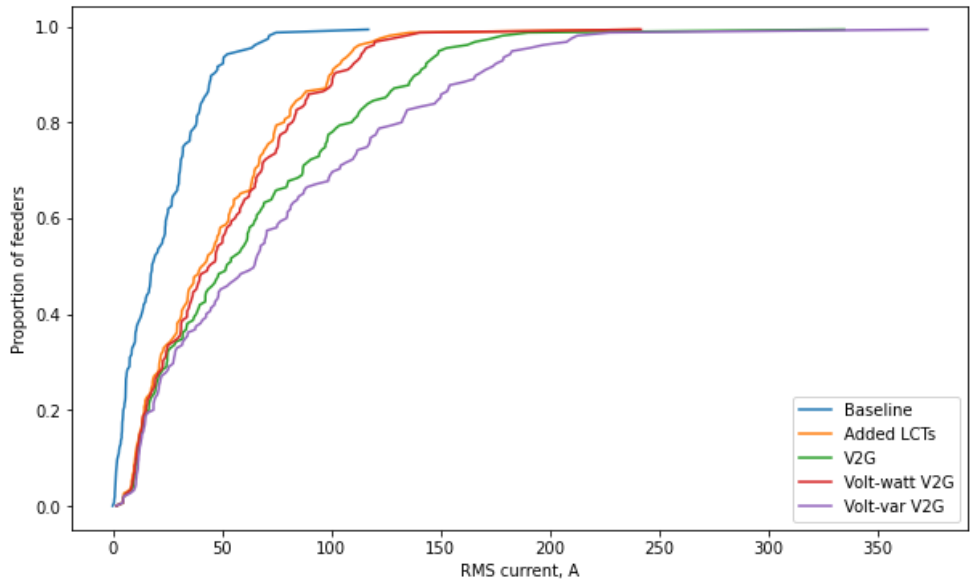

Figure 28: Maximum RMS substation currents per feeder, without diversified recharging

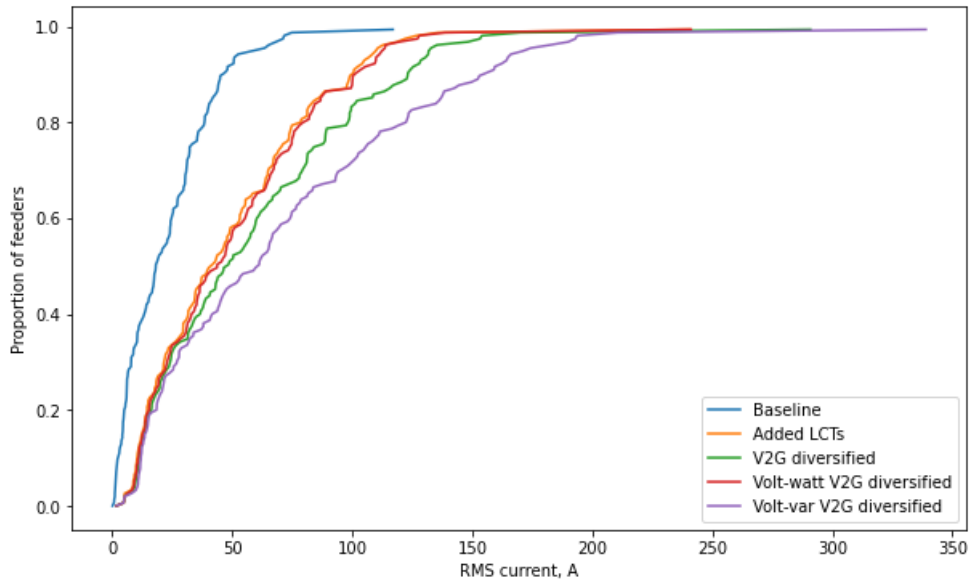

Figure 29: Maximum RMS substation currents per feeder, with diversified recharging

5.5 Mains branches with current overload

Figure 30 shows the proportion of branches on LV feeders with a current overload. This rarely occurs without V2G operation, and is mitigated by volt-watt control, although with a corresponding reduction in the exports provided. Volt-var control has minimal impact on the overloads.

Figure 31 shows the case where recharging is diversified, with over 80% of feeders having no overloads, compared to around 68% as above. However, the increased current with volt-var control causes a slightly greater incidence of overloads.

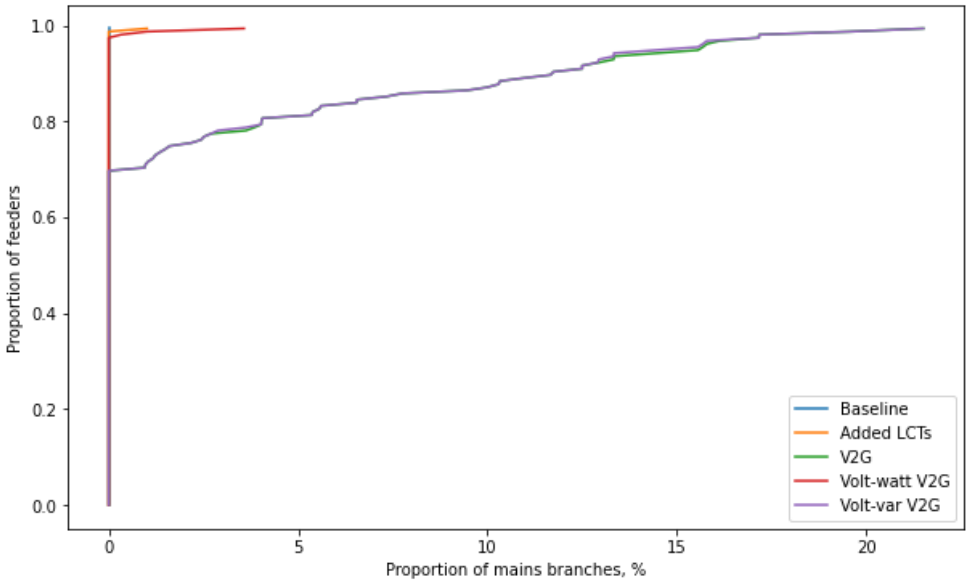

Figure 30: Mains branches with current overload, without diversified recharging

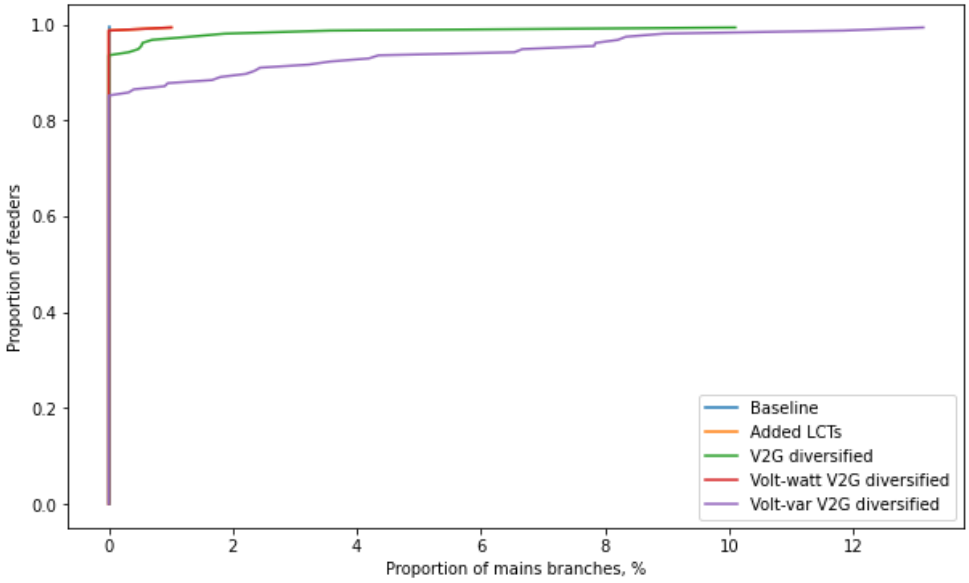

Figure 31: Mains branches with current overload, with diversified recharging

6. Conclusions

Simulations models have been developed to provide an initial review of the operation of volt-watt and volt-var control techniques.

These simulations have shown that volt-watt control methods can successfully reduce maximum voltages, peak currents and losses. The minimum voltages are also reduced, provided that the recharging following an export event is diversified. If recharging occurs simultaneously for all customers, significant voltage drops can occur as the recharging power import does not benefit from the same control as the V2G exports. Although volt-watt control is successful at mitigating the impact of V2G on the LV feeders, there is a reduction in the system benefit as less power can be exported.

Volt-var control also reduces the maximum voltage rise, but to a much lesser extent, and appears to have no positive impact on the worst-case voltage drop. Current amplitudes are increased by the reactive power consumed and so RMS currents at the substation are increased, as are mean losses.

From examination of individual substations, some high maximum voltages appear to be caused by increased phase unbalance, where increased neutral currents can cause the voltage on one phase to rise, even if there are reductions in load on the other phases.

The impact of volt-watt control can increase unbalance if voltages on one phase conductor are higher than on another, leading to an asymmetrical reduction in exports.

The model has so far assumed a constant power characteristic to represent the relationship between current and voltage at each connected appliance. This is a good approximation in many cases, but an improved model may be needed to represent the EV chargers. At present, if the voltage at a customer connection reduces, the model increases the current such that the desired power is delivered. This can further increase the voltage drop and could also oppose the impact of volt-var control.

Initial conclusions:

- Volt-watt control successfully reduces RMS substation currents and mean losses, although this is at the expense of a reduction in the overall level of exported power and so is undesirable from a system perspective, even if helpful in regard to LV capacity constraints.
- Volt-var control reduces worst-case voltage rise, but by a lesser extent than volt-watt control.
- Further work is needed to understand the impact of unbalance, as the control methods tend to operate asymmetrically where all the EV chargers on one phase have a higher voltage. This effect is accentuated by the non-linear nature of the ramped volt-watt and volt-var functions such that EV chargers on one phase may be fully constrained or not affected at all. The resulting unbalance can also lead to increased voltage deviations on other phases.
- The demand due to recharging has a significant impact on voltage ranges and could be a greater concern than the power exports, particularly where the rated import power is higher than the export power.
- A randomised delay has been proposed to mitigate the impacts of synchronised recharging. This would also need consideration in future volt-watt control standards.
- The impact of the constant-power load model needs further investigation.:
- Simulations so far have assumed a nominal substation busbar voltage of 245 V, based on previous experience of substation monitoring in the Losses Investigation. This voltage lies within the ramp range for volt-var control and so, some reactive power is consumed even in nominal conditions. Since reactive power is already being consumed in the nominal case, there is less additional reactive power than can be added when the voltage increases.

7. References

[1] Andrew Urquhart and Murray Thomson, “V2G Dynamic Headroom Control, Site Selection Report,” Loughborough University, 2025.

[2] Matthew Pope, “Standard Technique SD5H/1,” Sep. 2021.

[3] E. & I. S. Department for Business, “Subnational Electricity and Gas Consumption Statistics.” Accessed: Jun. 30, 2023. [Online]. Available: https://assets.publishing.service.gov.uk/government/uploads/system/uploads/attachment_data/file/1126284/subnational_electricity_and_gas_consumption_summary_report_2021.pdf

[4] National Grid Electricity Distribution, “Distribution Future Energy Scenarios (DFES).” Accessed: Mar. 05, 2025. [Online]. Available: https://connecteddata.nationalgrid.co.uk/dataset/dfes

[5] R. Lowe and Department of Energy and Climate Change, “Renewable Heat Premium Payment Scheme: Heat Pump Monitoring: Cleaned Data, 2013-2015,” UK Data Service. SN: 8151. Accessed: Jul. 19, 2023. [Online]. Available: https://beta.ukdataservice.ac.uk/datacatalogue/doi/?id=8151#!#1

[6] Ofgem, “Average gas and electricity use explained.” Accessed: Jun. 30, 2023. [Online]. Available: https://www.ofgem.gov.uk/information-consumers/energy-advice-households/average-gas-and-electricity-use-explained

[7] Energy Savings Trust, “Measurement of Domestic Hot Water Consumption in Dwellings.” [Online]. Available: https://assets.publishing.service.gov.uk/government/uploads/system/uploads/attachment_data/file/48188/3147-measure-domestic-hot-water-consump.pdf

[8] Stark, “Degree Days For Free.” Accessed: Oct. 20, 2023. [Online]. Available: https://poweredby.stark.co.uk/SEO/SEO.aspx

[9] I. Richardson and M. Thomson, “Integrated domestic electricity demand and PV micro-generation model,” 2011. [Online]. Available: https://dspace.lboro.ac.uk/2134/7773

[10] I. Richardson and M. Thomson, “Integrated simulation of photovoltaic micro-generation and domestic electricity demand: a one-minute resolution open source model,” in *Microgen II: 2nd International Conference on Microgeneration and Related Technologies, Glasgow, 4 - 6 April.*, Glasgow: © Microgen’II Organizing Committee, 2011. Accessed: Mar. 16, 2013. [Online]. Available: http://hdl.handle.net/2134/8774

[11] Western Power Distribution, “Electric Nation Customer Trial Final Report,” p. 591, 2019, [Online]. Available: https://www.westernpower.co.uk/downloads/64378

[12] M. Bognar, “Weibull distribution.” Accessed: May 01, 2021. [Online]. Available: https://homepage.divms.uiowa.edu/~mbognar/applets/weibull.html

[13] Andrew Urquhart and Murray Thomson, “V2G Dynamic Headroom Control, Control Algorithms Report,” Feb. 2025.

[14] SA Power Networks, “TS129 Small EG Connections Technical Requirements-Capacity not exceeding 30kVA,” 2021, Accessed: Jan. 20, 2025. [Online]. Available: https://www.sapowernetworks.com.au/public/download.jsp?id=318532